DEPARTMENT OF THE AIR FORCE
Contract AF 18 (600) -582

A STUDY OF TURBULENCE AND DIFFUSION USING TRACERS IN A WATER TUNNEL

Vito A. Vanoni
Norman H. Brooks

Hydrodynamics Laboratory
CALIFORNIA INSTITUTE OF TECHNOLOGY
Pasadena, California

January 31, 1955

Report No. E-46

Department of the Air Force
Contract AF 18(600)-582

A STUDY OF TURBULENCE AND DIFFUSION USING TRACERS IN A WATER TUNNEL

Vito A. Vanoni
Norman H. Brooks

Hydrodynamics Laboratory
California Institute of Technology
Pasadena, California

Report No. E-46

January 31, 1955

CONTENTS

		Page
I.	Abstract	1
II.	Introduction	2
III.	Theory of Turbulence and Diffusion	2
IV.	Apparatus and Experimental Procedure	7
	A. Water tunnel	7
	B. Experimental procedure	8
V.	Analysis of Plates	12
	A. Measurement of plates	15
	B. Magnification	15
	C. Flash frequency	16
	D. Standard error of calculated velocities	17
	E. Typical velocity curves for individual trajectories	18
	F. Calculation of average velocities for a set of trajectories	18
	G. Calculation of turbulence intensity	20
	H. Calculation of correlation coefficients	22
VI.	Outline of Experiments	24
VII.	Experimental Results	26
	A. Mean velocities	26
	B. Turbulence intensity and decay	31
	C. Lagrangian correlations	42
VIII.	Conclusions	48
IX.	Acknowledgments	50
	Bibliography	51

I. ABSTRACT

A study of turbulence in a water tunnel was made by observing the motion of small liquid droplets having the same density as water. These tracers were injected into the flow and their trajectories were photographed with a fixed camera using a stroboscopic light. From measurements of the photographic plates it was possible to calculate instantaneous velocities, turbulence intensities and Lagrangian correlation coefficients. Runs were made both with and without a turbulence-producing grid; three geometrically similar grids were used. From 11 to 35 separate trajectories were measured for each run. Each point value of the turbulence characteristics is an ensemble average.

The biggest limitation on the practical application of this method is the inevitable sampling error in the calculated intensities and correlations. These errors were large, even when 35 trajectories were measured; they can be reduced only by greatly increasing the number of trajectories analyzed. A satisfactory experimental technique for photographing and measuring the trajectories of the tracers was developed, but the computations are still very laborious.

The results of the study showed that a large fraction of the turbulent energy of the field may be attributed to substantial differences between the mean velocities of different tracers over the 3-ft observation reach. The decay of turbulence energy with distance showed a linear relation between the reciprocal of the energy and the distance, as has been previously found, but a strong Reynolds number effect was observed.

The correlation curves indicated that the time scale was fairly large, and it appeared that practically all the energy was associated with relatively low frequencies. Unfortunately, the data were not extensive enough to permit calculation of the diffusion coefficients from the Lagrangian correlations in accordance with Taylor's theory.

II. INTRODUCTION

Diffusion in a liquid is caused by molecular motion and by turbulence. In a turbulent flow it is well known that the effect of the turbulence is many times that of the molecular motion, so that the latter can be neglected by comparison. The study of diffusion in a turbulent flow then is actually a study of the diffusion properties of turbulence, or simply a study of turbulence. Most observations of turbulence have been made by means of instruments that are fixed in the flow field, thus yielding data in the Eulerian coordinate system. In diffusion studies one is interested in the transport of particles of fluid or other matter in the fluid which is best observed in the Lagrangian frame of reference. Studies of the motion of such particles are of interest since they yield information on turbulence of which there is a scarcity.

When this project was authorized in the spring of 1953, a water tunnel was available in which to make the necessary experiments. The tunnel had been built for making turbulence and diffusion studies but it had not been used for this purpose so that its characteristics were not known. Therefore the objective of the study included not only the investigation of properties of a turbulent water flow but also determination of characteristics of the tunnel and the exploration of its suitability for carrying out turbulence studies.

III. THEORY OF TURBULENCE AND DIFFUSION

Properties such as heat and momentum, and foreign matter such as dust particles are diffused in a turbulent fluid in much the same way as molecules and particles in Brownian motion. In the theory of molecular diffusion the basic assumption is made that the rate of transport n of a property with concentration N is proportional to the gradient of the concentration N. For a one-dimensional case this relation is

$$n = -D \frac{dN}{dx} \tag{1}$$

where in this case n is the rate of transport of the property in the x direction per unit time and unit area, and D is the diffusion coefficient. In the most general case considered, N is a function of time and space and

D is a function of space only. The diffusion equation in this general case is

$$\frac{DN}{Dt} = \frac{\partial}{\partial x}\left(D_1 \frac{\partial N}{\partial x}\right) + \frac{\partial}{\partial y}\left(D_2 \frac{\partial N}{\partial y}\right) + \frac{\partial}{\partial z}\left(D_3 \frac{\partial N}{\partial z}\right) \tag{2}$$

where $\frac{DN}{Dt} = \frac{\partial N}{\partial t} + U\frac{\partial N}{\partial x} + V\frac{\partial N}{\partial y} + W\frac{\partial N}{\partial z}$,

in which U, V, and W are components of fluid velocity and D_1, D_2, and D_3 are the diffusion coefficients in the x, y, and z directions, respectively.

In order to solve the diffusion equation (Eq. 2), it is necessary to evaluate D. In the self diffusion of gases, Jeans (Ref. 1) derived the diffusion coefficient D as

$$D = \frac{1}{3}\,\bar{c}\,L$$

where $\bar{c}$ is the mean velocity of the gas molecules and L is their mean free path. For the case of Brownian motion, Einstein (Ref. 2) has expressed the diffusion coefficient by

$$D = \frac{1}{2}\,\frac{\overline{Y^2}}{T} \tag{3}$$

where $\overline{Y^2}$ is the mean-square displacement of the particles in the y-direction during an interval of time T, and where T is sufficiently long so that velocities at the beginning and end of the interval are uncorrelated. Taylor (Ref. 3) has developed a theory for diffusion in turbulent flow which gives a result similar to the Einstein equation (Eq. 3) as will be shown below.

To study the problem of turbulent diffusion one considers the motion of foreign particles having the same density as the fluid and a size sufficiently small so that their motion will reveal the details of the turbulent fluid motion without disturbing it. If there is a mean motion of the fluid, it is assumed to be steady, rectilinear and uniform over the field. By introducing a coordinate system moving with the mean velocity, one can eliminate its effect and study only the turbulent motion. In general, turbulent motion occurs in all three coordinate directions. For convenience, only one component of the motion will be dealt with.

Following Burgers (Ref. 4), the y component of the displacement in

time T of a particle is

$$y = \int_o^T v'(t_o, T')\, dT'$$

where $v'(t_o, T')$ is the turbulent fluctuation of the instantaneous velocity v at time $t_o + T'$, t_o is the value of the time when observations start, and, as stated above, T is the time interval over which observations are made. One can now write,

$$y^2 = \int_o^T dT' \int_o^T v'(t_o, T')\ v'(t_o, T'')\, dT'' \tag{4}$$

where $v'(t_o, T'')$ is the velocity of the particle under observation at time $t_o + T''$. By observing a large number of such particles, one can obtain the mean-square deviation of the y-displacement,

$$\overline{y^2} = \int_o^T dT' \int_o^T \overline{v'(t_o, T')\ v'(t_o, T'')}\, dT'' \tag{5}$$

where the bar denotes mean value for all t_o values. If the turbulent motion is assumed to be stationary with respect to time and homogeneous in space, the mean product $\overline{v'(t_o, T')\ v'(t_o, T'')}$ is an even function of time difference $\tau = T'' - T'$ only.

From the definition of correlation coefficient in statistics one can write the expression for the correlation coefficient r_v between velocity fluctuations,

$$r_v(\tau) = \frac{\overline{v'(t_o, T')\ v'(t_o, T'')}}{\overline{v'^2}} \tag{6}$$

Substituting Eq. 6 into Eq. 5 gives

$$\overline{y^2} = \overline{v'^2} \int_o^T dT' \int_o^T r_v(\tau)\, dT'' \ . \tag{7}$$

Since $\tau = T'' - T'$ and $r_v(\tau)$ is an even function, the integrated integral of Eq. 7 can be reduced to a simple integral over τ with the result,

$$\overline{y^2} = 2\,\overline{v'^2}\,T \int_0^T r_v(\tau)\,d\tau - 2\,\overline{v'^2} \int_0^T \tau\, r_v(\tau)\,d\tau \tag{8}$$

The integrals in Eq. 8 may be expected to approach constant values when T becomes large because $r_v(\tau)$ must become zero for sufficiently large values of τ. Let these be donated as

$$\overline{v'^2} \int_0^T r_v(\tau)\,d\tau = D \tag{9}$$

and

$$\overline{v'^2} \int_0^T \tau\, r_v(\tau)\,d\tau = D\,T_o \tag{10}$$

Then for large T, Eq. 8 will take the form

$$\overline{y^2} = 2D(T - T_o) \tag{11}$$

or

$$D = \frac{\overline{y^2}}{2(T - T_o)} \tag{12}$$

which is similar to Eq. 3 for Brownian motion. If Eq. 2 is solved for the one-dimensional problem of diffusion from a point source in a homogeneous isotropic field, it may be shown that the Fickian diffusion coefficient defined by Eq. 1 is identical to Einstein's value of D in Eq. 3, and only slightly different from D in Eq. 12.

It is evident from Eq. 9 that the diffusion coefficient in the y-direction can be calculated from measurements of the correlation coefficient $r_v(\tau)$. Similar relations can be derived between diffusion coefficients in the x- and z-directions and the correlation functions $r_u(\tau)$ and $r_w(\tau)$. In a homogeneous isotropic field of turbulence the three functions $r_u(\tau)$, $r_v(\tau)$, and $r_w(\tau)$, as well as the the three corresponding diffusion coefficients, are theoretically identical. Such correlation functions referring to the history of individual particles are known as Lagrangian correlation coefficients.

Extensive studies (Refs. 5, 6, 7, 8) of isotropic turbulence produced by grids in wind tunnels have shown that the root-mean-square velocity

fluctuations $\sqrt{\overline{u'^2}}$ and $\sqrt{\overline{v'^2}}$ in the longitudinal and transverse directions are the same. Measurements of the turbulent energies $\overline{u'^2}$ and $\overline{v'^2}$ all show that they decay with distance from the generating grid. Dryden (Ref. 5) found that such measurements made at the U. S. National Bureau of Standards followed a linear relationship between $U^2/\overline{u'^2}$ or $U^2/\overline{v'^2}$ and x, where x is the distance downstream from the grid and U is the mean velocity in the tunnel. This relationship was confirmed (Ref. 7, 8) by measurements at Cambridge University for values of x that are not too large. For geometrically similar grids the relation (Ref. 8)

$$\frac{U^2}{\overline{u'^2}} = a\left(\frac{x}{M} - \frac{x_o}{M}\right) \tag{13}$$

has been found to apply where M is the mesh size of the grid, x_o is a constant, and the factor "a" depends principally on the shape of the grid, although it may also vary slowly with the grid Reynolds number, UM/ν, where ν is the kinematic viscosity of the fluid. Equation 13 was found to apply for values of x/M less than about 200. The time required for the flow to traverse this distance is called the initial period. Beyond this initial period the dissipation is more rapid than that given by Eq. 13.

A more general relation (Ref. 7) for decay in the initial period is

$$\frac{U^2}{\overline{u'^2}} = \frac{b}{C_D}\left(\frac{x_o}{M} - \frac{x_o}{M}\right) \tag{14}$$

where $C_D\ \rho U^2/2$ is the drag force which a unit cross-sectional area of the grid exerts on the stream and ρ is the mass density of the fluid. Values of b in Eq. 14 were found to vary from 90 to 128 for data obtained with square mesh grids with ratios of M to rod diameters d from 2.16 to 5.33. In obtaining these values of b, C_D was calculated from the following empirical formula

$$C_D = \frac{\frac{d}{M}\left(2 - \frac{d}{M}\right)}{\left(1 - \frac{d}{M}\right)^4} \tag{15}$$

IV. APPARATUS AND EXPERIMENTAL PROCEDURE

A. Water Tunnel

The water tunnel used in the present experiments has been described in detail (Refs. 9, 10) elsewhere, so that only a brief description will be given here. A photograph of the tunnel is shown in Fig. 1, and a diagram of the flow circuit is shown in Fig. 2.

The working section, which is 105-3/8 in. long, is 12 in. x 12 in. in cross section at the upstream end and 12 in. wide x 14 in. high at the downstream end. It is divided into two panels of equal length by thin struts at mid span. The side windows, which are of 1-1/4-in. thick plate glass, are parallel to each other and 12 in. apart. The top and bottom windows are of lucite and are removable to permit access to the working section.

The nozzle upstream from the working section is square in cross section, being 46 in. x 46 in. at the inlet end and 5 ft long. Upstream from the nozzle is a prismatic section 46 in. x 46 in. in cross section and about 4 ft long, which contains three turbulence damping screens woven of 0.018-in. diameter wire with 18 meshes to the inch. A sheet metal honeycomb baffle with equilateral triangular passages about 1 in. in altitude and 7 in. long is located at the upstream end of the prismatic section. The first two vane elbows upstream from the nozzle are also 46 in. x 46 in. in cross section, and differ only in the size and number of turning vanes at the corners. The vanes in the first elbow upstream have a spacing of about 1 in. and a chord length of 2-7/8 in. Those in the second elbow are spaced at 3-7/8 in. and have a chord length of 11 in. The flare angles of the diffusers (downstream from the working section and in the return pipe) are small, being about 5 degrees, or less, so that there is little likelihood of separation in the flow.

The water is circulated by a 30-in. pump of the mixed flow type which has a maximum efficiency of 88 percent. The pump is driven by a 30 h.p. direct current motor through a vee-belt transmission. The water velocity in the working section is controlled by the motor speed, which is in turn controlled by varying the field current. This is done automatically by a device (Ref. 11) by means of which the speed of the pump can be set and maintained at any predetermined value. The flow velocity is indicated by the pressure drop across the nozzle, which was read with a water-air

manometer.

In order to take satisfactory photographs it was necessary to keep the water clean. The principal device for accomplishing this was a filter which employs diatomaceous earth on cylindrical porous stones as the filtering elements. The filter, which had a capacity of about 30 gallons per minute, was on a by-pass circuit in parallel with the lower portion of the tunnel circuit and was operated almost continuously when the program was in progress.

A good coating of vinyl resin paint on the interior of the steel surfaces of the tunnel circuit prevented rusting and aided materially in keeping the water clean. The galvanized corrugated sheet iron tank at the right of Fig. 1 was used to store water drained from the tunnel when it was necessary to open up the working section for any purpose. By keeping this tank clean, water stored in it remained clean.

B. Experimental Procedure

The turbulence in the working section was produced artificially by square mesh grids of circular rods located at the throat of the nozzle, i.e., at the inlet to the working section, as shown in Fig. 3. The vertical rods were downstream from the horizontal rods and the two sets were in contact with each other. Three grids with mesh distances of 1/2, 1 and 2 inches were used. In all grids the mesh distance was four times the rod diameter. At the four walls of the working section a half rod was used to maintain the grid pattern.

The data taken in these experiments consist of observations of the positions of tracer particles in the flow as a function of time as they move across the working section. The location of a particle at various points in its trajectory was determined by taking a multi-exposure photograph of the particle on a single plate as it traversed the field of the camera. The photographs were taken stroboscopically with a lamp which was flashed at a known constant frequency, thus making it possible to determine the time interval between any two positions of a tracer particle. The local instantaneous velocity was determined from this time and the distance between tracer positions obtained from measurements on the plate.

The tracers were droplets of a mixture of carbon tetrachloride and mineral oil colored white with a small amount of zinc oxide added in paste

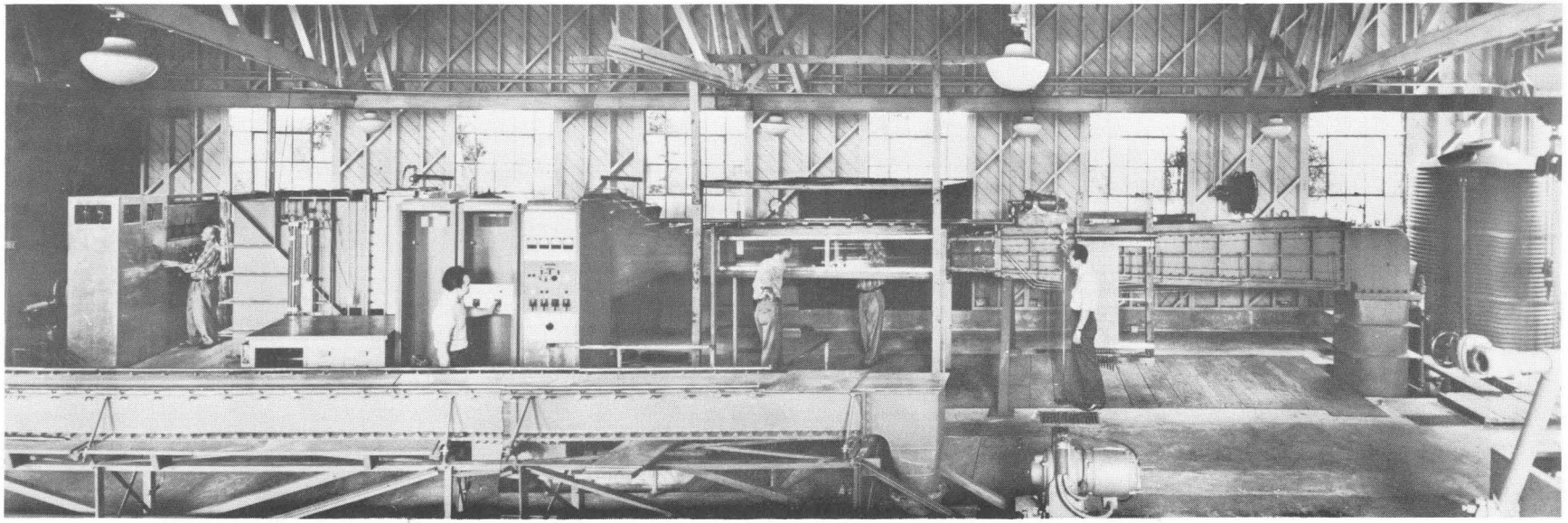

Fig. 1 - Photograph of water tunnel.

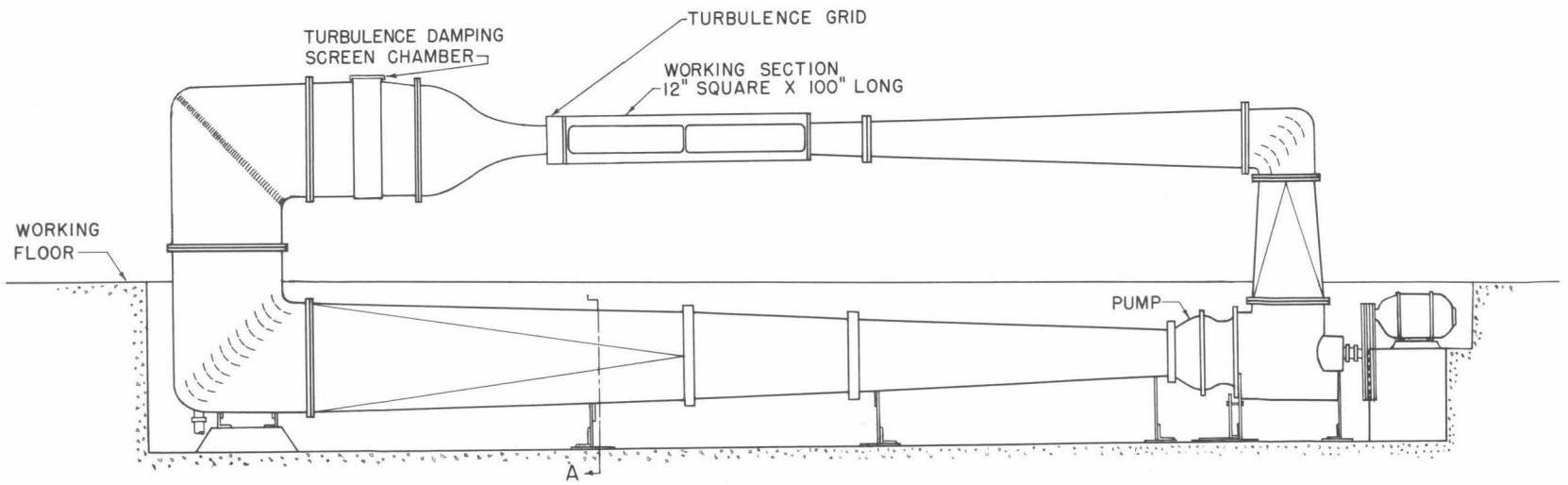

Fig. 2 - Diagram of flow circuit of water tunnel.

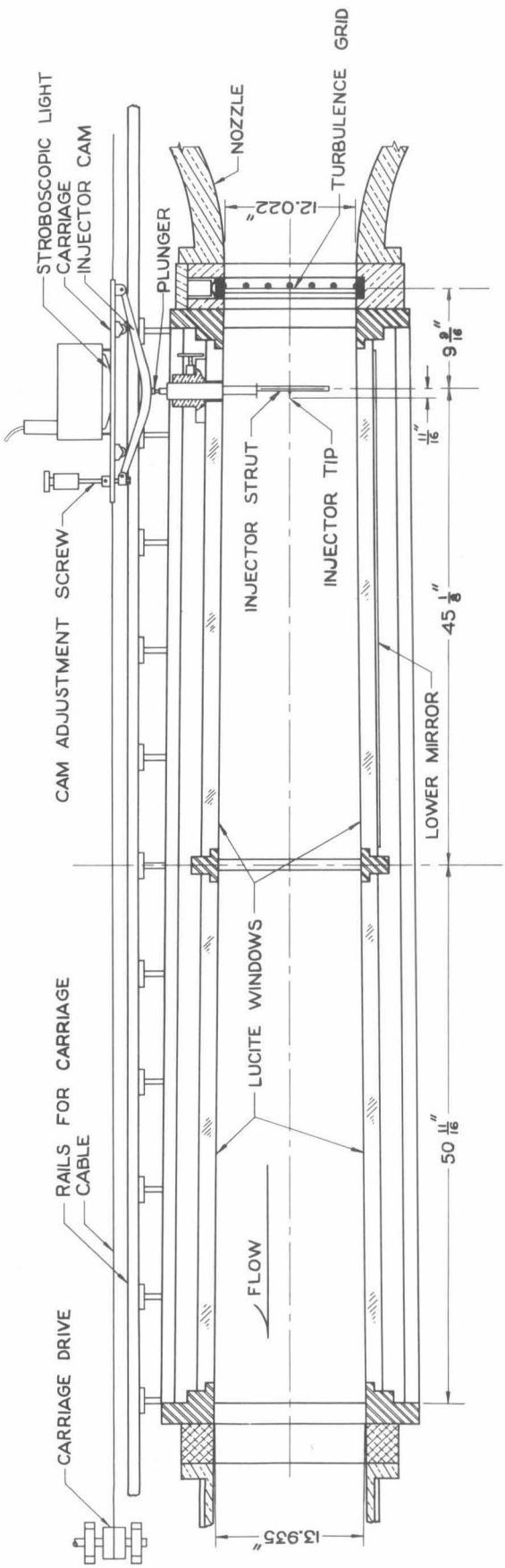

Fig. 3 - Centerline profile of the working section of the tunnel showing turbulence grid, strut for tracer injector, and carriage for stroboscopic light.

form. The proportions of the three ingredients were adjusted by trial so a droplet of the tracer liquid would neither rise nor settle in a sample of the tunnel water. The liquid was injected into the tunnel working section through a very small tube. As the liquid was injected it broke up into droplets ranging from 0.3 to 1.0 mm in diameter, which were easily seen and photographed. Only enough liquid was injected at one time to make not more than about four droplets.

Two injector systems were used. One of these, referred to as the strut injector, is shown diagrammatically in Fig. 3. The injector tube is carried inside a compound strut extending down from the top window with the tip, which is at the center of the cross section, protruding 1/2 inch downstream from the trailing edge of the strut. Both sections of the strut are streamlined. The upper section has a chord of 3/4 in. and a thickness of 1/8 in., and the lower section has a chord and a thickness of 0.42 in. and 0.07 in., respectively. Originally the lower strut stopped 5/16 in. below the injector tip, but was later extended an additional 3-5/16 in. The two sections of strut are separated by a disk 1-15/32 in. in diameter that has a sharpened edge.

To control the droplet size, several sizes of outlet tip were used ranging from 0.010 to 0.078 in. in inside diameter. The outside of each tube was tapered to make a sharp edge at the tip.

The second injector system was built into the center vertical rod of the turbulence-producing grid. The injector tips described above were fastened directly to the center rods, so that practically no disturbance was created by the injector.

Figure 3 also shows the stroboscopic light used to take the pictures. The light was mounted on a carriage which was pulled along the working section at the same velocity as the flow, so that it remained over the cluster of tracer droplets injected into the tunnel. In this way only a small part of the field was ever illuminated at one time, and thus fogging of the film due to light scattered by the water was kept at a minimum.

An adjustable cam attached to the carriage, and also shown in Fig. 3, forced a small piston into the injector as the carriage moved forward and injected the desired amount of tracer liquid right under the light. The lower mirror, shown in Fig. 3, was placed face up under the lower window

to light the under side of the tracers by reflected light.

Figure 4 shows a plan and profile view of the optical system used to record the positions of the tracers. The camera consisted of a process lens with a focal length of 9.5 in. and a maximum relative aperture of f 9 mounted in a simple rigid box. The camera assembly was mounted rigidly on a bracket attached to the building frame. Glass photographic plates 5 x 7 in. in size were used to facilitate the measurements. The entire working section and the camera used to take the photographs were housed in a light-tight enclosure. The two posts at the ends of the working section, shown in Fig. 1 , are part of the framing for the enclosure and indicate its size.

As shown in Fig. 4, two views of the tracers were taken simultaneously on a single plate. One was a profile view in a vertical plane and showed the longitudinal and vertical motions. The other was taken through the mirror and was an oblique view looking diagonally downward. The latter view was used to determine the horizontal distance of the tracer from the center of the working section with sufficient accuracy to determine the magnification factor or the ratio of distances in the tunnel to corresponding distances on the plate. No transverse velocities were determined from measurements of the oblique photograph since the tracer positions determined from them were not sufficiently accurate for this purpose.

V. ANALYSIS OF PLATES

Each plate is a stroboscopic photograph of the motion of one or more tracer droplets in the turbulent flow field. The trajectories are recorded in both direct and mirror views by about 120 separate exposures of the tracer as it crosses the field of view. Figure 5 shows enlarged views of three typical trajectories on a single plate. To save space, only the trajectories themselves have been reproduced, although the original plate shows the fiducial marks and the sides of the tunnel.

From precise measurements of the plates it was possible to determine the instantaneous velocities of the tracers at any time; with these velocities, turbulence intensities and correlations were then calculated. The procedure for making these measurements and calculations will be outlined below.

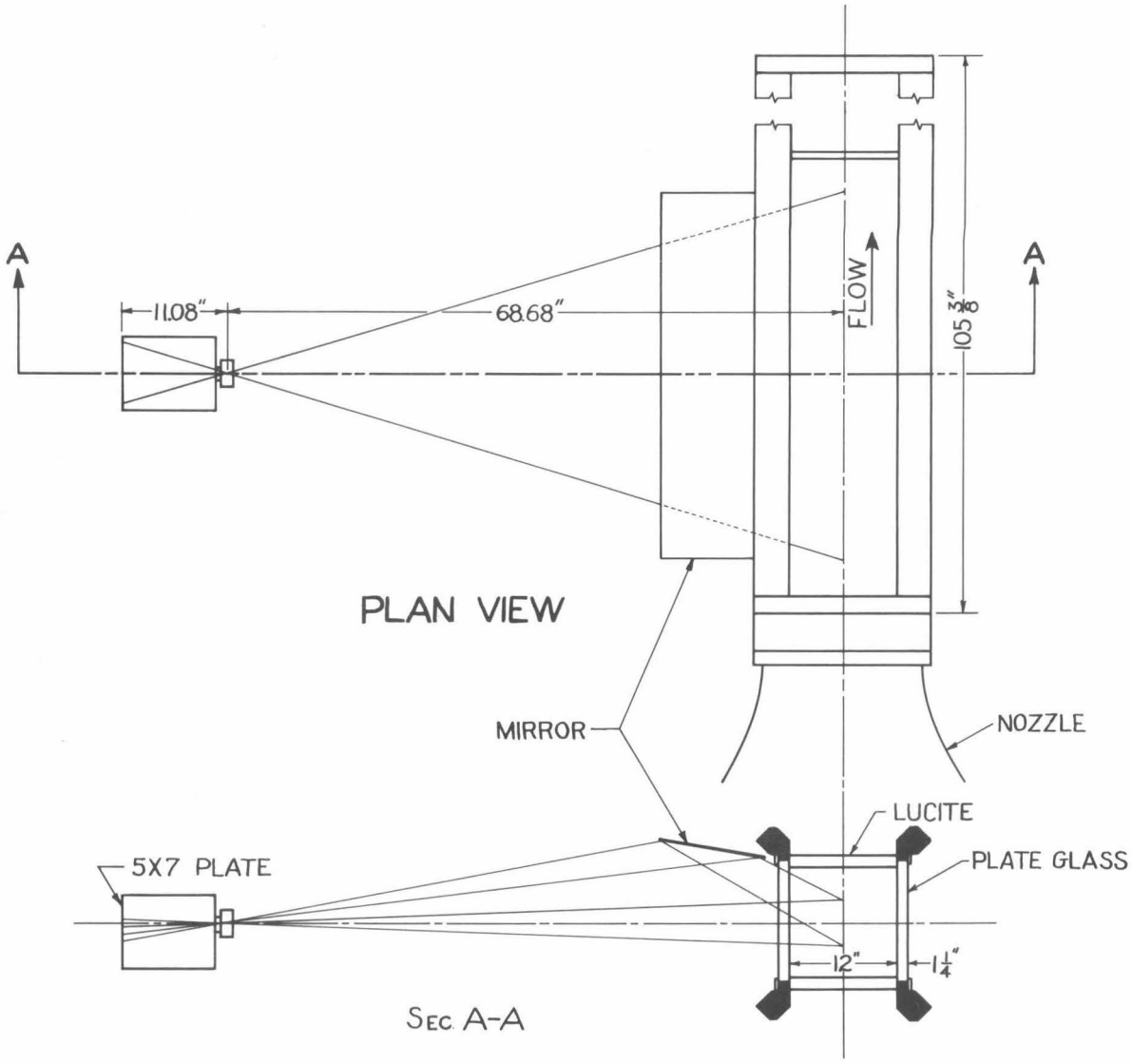

Fig. 4 - Diagram of optical system for photographing tracers.

Fig. 5 - Typical photograph of trajectories of tracers (printed as a negative). (a) Mirror view; (b) direct view; (c) enlarged view of a section of (b). Views (a) and (b) have been enlarged about 1.5 times from the photographic plate, while view (c) is about twice the actual in the tunnel.

A. Measurement of Plates

The positions of the droplet images on the plates were measured with a micro-comparator, an accurate two-dimensional optical measuring device. A coordinate system on the plate was established by the images of three fiducial marks on the front window of the tunnel working section. On the direct view both longitudinal and vertical positions were measured, and in the mirror view the vertical position was measured in order to obtain the transverse position in the tunnel. In the longitudinal direction the comparator scale is graduated in microns and in the vertical direction in tens of microns (0.01 mm). Both scales were read to the nearest micron.

An estimate of the accuracy of the plate measurements was obtained by having each observer make 50 repeated measurements of the position of a few selected representative images. The standard error (or standard deviation) of the measurements by each observer was found to be about 2.5 microns in the longitudinal direction and 3.1 microns in the vertical direction. This error is due in part to the difficulty of setting the cross hairs precisely in the center of the tracer image, which usually ranged in size from about 50 to 150 microns (droplet diameter 0.3 to 1.0 mm in tunnel). Systematic differences in reading by different observers were of no importance because each plate was analyzed entirely by one observer, and the velocities are determined from the changes of position between images.

B. Magnification

There were two factors which made it necessary to apply a varying magnification factor to the measured plate distances to obtain actual distances in the tunnel. First, the tracers after being diffused were at varying transverse positions in the tunnel, and hence at varying optical distances from the camera. When a tracer is in front of the tunnel centerline, a given displacement in the tunnel appears larger on the plate, thus making the magnification ratio smaller; and for droplets behind the centerline the opposite is true. Secondly, the refraction of the light rays by the water and the glass window introduces a distortion such that a plane in the tunnel perpendicular to the optical axis no longer appears flat. The water shortens the optical path for all points but the effect is greatest near the edges of the field of view. Thus, the ends of an imaginary axial line in the tunnel appear to be bent toward the camera, giving magnification ratios less at the ends than at the center.

The corrections for these factors, and also for any small errors in the construction and alignment of the camera, were determined experimentally using a steel plate with carefully scribed grid lines at 1/2-in. intervals. The grid was placed vertically in the working section and photographed in three different positions (along the centerline and 2 in. to each side) with the same optical setup later used to obtain data. From measurements on the photographs of the grid it was possible to find the magnification ratio as a function of the actual position in the tunnel. Since the position of a point in the tunnel can be uniquely determined from the direct and mirror views on the photographic plate, the magnification ratio could therefore be expressed directly as a function of the measured coordinates on the plate.

The magnification ratio thus obtained did not vary greatly. In moving along the axis of the tunnel, the ratio ranged from 6.043 at the center (on the optical axis) to 6.027 at a point 15 in. upstream from the center, and 6.033 at a point 15 in. downstream from the center. On the optical axis, the magnification 2 in. in front of the centerline was 5.906 and 2 in. behind the centerline was 6.168. The variation of the magnification ratio with the vertical position in the tunnel was negligible because of the small range of vertical coordinates. The standard error in the magnification charts prepared for use in reducing the data is estimated to be not more than 0.2%.

In analyzing the trajectories on the photographic plates, the longitudinal and vertical displacements between adjacent tracer images in the direct view are multiplied by the magnification factor to determine the corresponding actual differential displacements in the tunnel. The measured position in the mirror view is used only in obtaining the magnification factor, as the accuracy is not sufficient to justify calculation of transverse differential displacements in the tunnel.

C. Flash Frequency

If Δx and Δy are the measured components of the distance between two adjacent images on a photographic plate, the longitudinal and vertical velocities u and v may be calculated from the equations

$$u = mf\,\Delta x, \quad \text{and} \quad v = mf\,\Delta y$$

where m is the magnification ratio and f is the flash frequency of the stroboscopic lights. The velocity components thus obtained represent averages during the time interval 1/f between flashes.

The flash frequency used was 60 cps for nominal mean velocities of 50 cm/sec and 180 cps for nominal mean velocities of 150 cm/sec. The frequency was carefully checked against the powerline frequency with a cathode ray oscilloscope during experimental runs. The error in the line frequency is reasonably assumed to be less than 0.1%.

An experimental determination of the uniformity of flash intervals was made by measurements of a stroboscopic photograph of a high-speed rotating disc with a reference mark. The study showed that the standard deviation of the time intervals was only 0.05% of the mean.

All of the calculations were made on a calculating machine with enough digits to insure that no further significant errors were introduced.

D. Standard Error of Calculated Velocities

The over-all standard error in the velocity measurement may be found in the following way. First of all, it may be shown from statistics that for normally distributed variables the variance (standard deviation squared) of a sum or difference of several variables is equal to the sum of the variances for the individual variables. Thus the standard error for the distance Δx between two tracer images is $\sqrt{2.5^2 + 2.5^2} = 3.5$ microns, because Δx is a difference between two plate measurements. For a typical Δx of 1300 microns, the percentage standard error is then 0.27%.

Since for any individual calculation the percentage errors from all sources (Δx, m, f) are additive, the standard error (or standard deviation) is found by applying the same rule again. Hence, if the standard errors for horizontal distance on the plate (Δx), magnification (m), and flash frequency (f) are 0.27%, 0.2% and 0.15%, respectively, the total standard error in the velocity u will be approximately

$$\sqrt{0.27^2 + 0.2^2 + 0.15^2} = 0.4\%.$$

This figure corresponds exactly to the apparent turbulence intensity of u ($\sqrt{\overline{u'^2}}/U$) which the calculations would show even if there were absolutely no turbulence.

A similar calculation for the vertical velocity, v, shows that the ratio of the standard error for v to the mean forward velocity is also approximately 0.4%; furthermore, this figure represents the apparent $\sqrt{\overline{v'^2}}/U$ in the complete absence of turbulence.

It should be noted that the above discussion is confined only to the errors introduced in the analysis of the photographic plates. There are undoubtedly other sources of error, such as slight fluctuations in mean tunnel velocity and slight nonuniformity of tracer density, which will increase the values of the apparent turbulence intensities for u and v, respectively.

E. Typical Velocity Curves for Individual Trajectories

By the procedure outlined above, two components of velocity may be found for each flash interval of a trajectory. For convenience, a time scale t was established for each trajectory in such a way that time t = 0 fell (within a fraction of a flash interval) at a prescribed position just slightly downstream from the center of each plate. Since the turbulence intensity was always low, the value of t is closely related to the distance x from the grid by the approximate equation

$$x \doteq Ut + x_1 \tag{16}$$

where U is the average velocity of flow and x_1 is the distance to the t = 0 position.

The variation of the longitudinal and vertical velocities with time t for three trajectories on plate No. 612 (Set VI, trajectory Nos. 1, 2 and 3) is shown in Fig. 6. The grid is located at approximately t = − 100/60 sec.

F. Calculation of Average Velocities for a Set of Trajectories

When a group of trajectories in the same flow are analyzed, there are several ways to calculate average velocities. Let $u_i(t)$ and $v_i(t)$ be the longitudinal and vertical velocity components at time t (as defined above) for the i^{th} trajectory of a set; $\overline{u}(t)$ and $\overline{v}(t)$ will then be used to designate the average velocities for the whole set of trajectories at a particular value of t. The average velocities for each of the individual trajectories will be denoted by $\overline{u}_i$ and $\overline{v}_i$; since it is laborious to calculate $\overline{u}_i$ and $\overline{v}_i$ by integrating over all t values, and since the quantities are of secondary importance in the analysis anyway, only approximate values of $\overline{u}_i$ and $\overline{v}_i$ were found by averaging the velocities calculated for every sixth flash

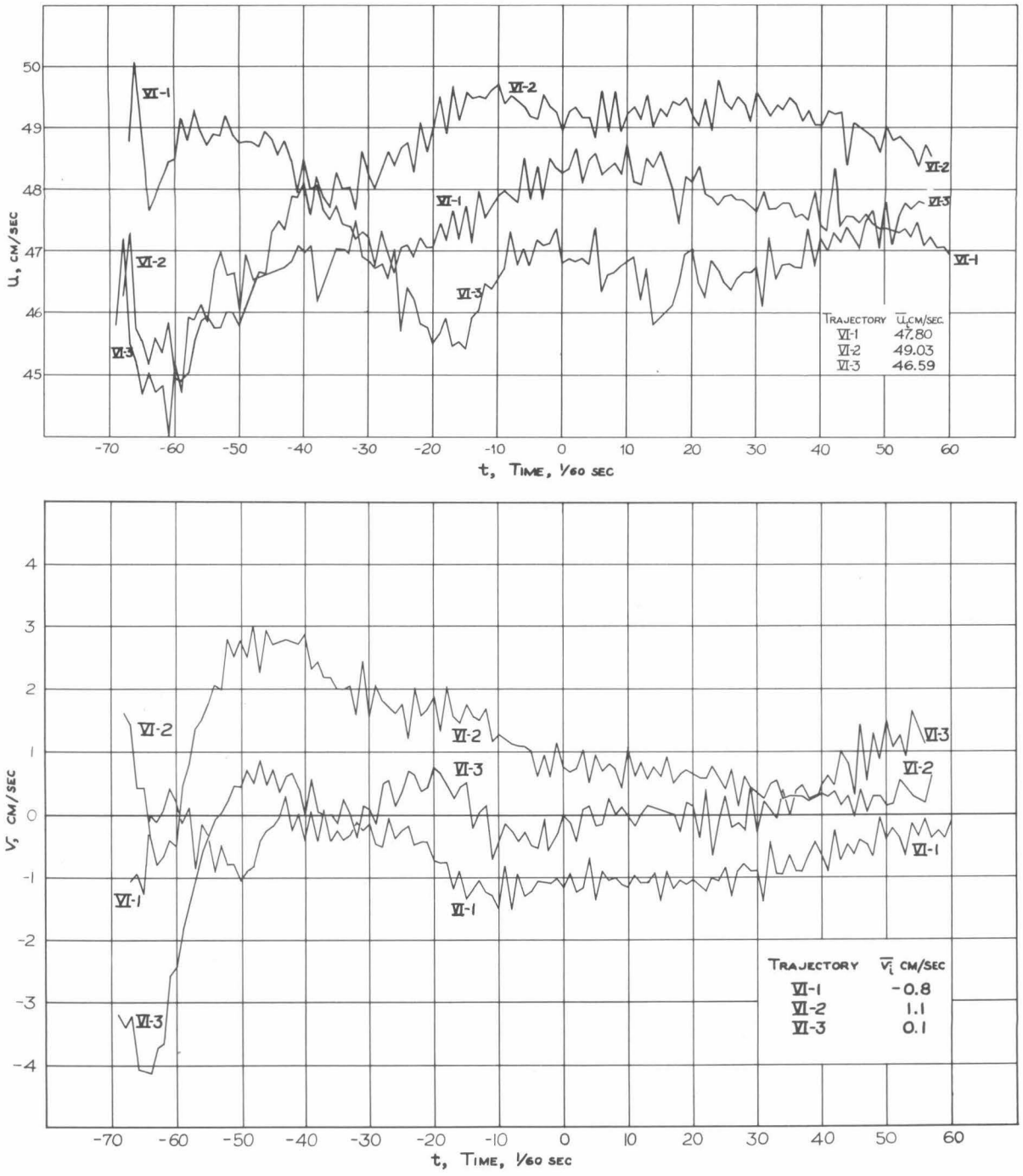

Fig. 6 - Instantaneous longitudinal and vertical velocities, u and v, as functions of time for three typical trajectories on a single photographic plate (Set VI).

interval. Since this scheme uses 15 values of t, the averages $\overline{u}_i$ and $\overline{v}_i$ will henceforth be referred to as the 15-point average trajectory velocities. By detailed calculations for one set of trajectories it was found that the 15-point averages were very close to the true averages.

The over-all averages, calculated either as the 15-point averages of $\overline{u}(t)$ and $\overline{v}(t)$ or as the set averages of $\overline{u}_i$ and $\overline{v}_i$ will be designated as U and V. The various averages for all sets are given in graphical or tabular form in Section VII, A.

The random experimental errors will be largely cancelled out in the averaging process but there may still be substantial sampling errors, as will be discussed in Section III, A.

G. Calculation of Turbulence Intensity

As in the case of calculating mean velocities, the calculation of turbulence intensities can be done in several ways. First, for any particular value of the time t, the intensities were calculated from the ensemble of trajectories by the formulas

$$\sqrt{\overline{u'^2}} = \sqrt{\frac{n}{n-1}\left[\overline{u_i(t)^2} - \overline{u}(t)^2\right]}, \tag{17}$$

$$\sqrt{\overline{v'^2}} = \sqrt{\frac{n}{n-1}\left[\overline{v_i(t)^2} - \overline{v}(t)^2\right]}, \tag{18}$$

where the bar designates average value for all trajectories. Since the decay was appreciable, it was considered desirable to calculate these intensities as functions of t (or of the corresponding distance from the grid x).

The variable mean velocity $\overline{u}(t)$ was used in this calculation in preference to the over-all average U. Had U been used, the calculated turbulence intensities would have been too large, since the minimum values of intensity are obtained using the sample means $\overline{u}(t)$. To be consistent, $\overline{v}(t)$ was also used. The factor $\frac{n}{n-1}$, where n is the number of trajectories in the set, is included for statistical reasons so that an unbiased estimate of the intensities may be obtained when the samples are not very large.

In addition, some calculations of turbulent energies by other means were made to clarify the effects of various factors. The following quantities may be calculated:

Over-all energy: (based on all trajectories in a set and 15 values of t)

$$E = \overline{\overline{u_i(t)^2}} - U^2 \tag{19}$$

$$F = \overline{\overline{v_i(t)^2}} - V^2 \tag{20}$$

Energy for a position t : (based on all trajectories in a set)*

$$E(t) = \overline{u_i(t)^2} - \overline{u}(t)^2 \tag{21}$$

$$F(t) = \overline{v_i(t)^2} - \overline{v}(t)^2 \tag{22}$$

Energy for $i^{\underline{th}}$ trajectory: (based on 15 values of t)

$$E_i = \overline{u_i(t)^2} - \overline{u}_i^2 \tag{23}$$

$$F_i = \overline{v_i(t)^2} - \overline{v}_i^2 \tag{24}$$

Variance for position averages of velocity: (based on 15 values of t)

$$\sigma^2_{\overline{u}(t)} = \overline{\overline{u}(t)^2} - U^2 \tag{25}$$

$$\sigma^2_{\overline{v}(t)} = \overline{\overline{v}(t)^2} - V^2 \tag{26}$$

Variance for average velocities of trajectories: (based on all trajectories in a set)

$$\sigma^2_{\overline{u}_i} = \overline{\overline{u}_i^2} - U^2 \tag{27}$$

$$\sigma^2_{\overline{v}_i} = \overline{\overline{v}_i^2} - V^2 \tag{28}$$

Some of the bars indicate average over t, and others average over i trajectories, as indicated in the headings at the left. The following identities may be readily verified by algebra:

$$E = \overline{E_i} + \sigma^2_{\overline{u}_i} = \overline{E(t)} + \sigma^2_{\overline{u}(t)} . \tag{29}$$

$$F = \overline{F_i} + \sigma^2_{\overline{v}_i} = \overline{F(t)} + \sigma^2_{\overline{v}(t)} . \tag{30}$$

It will be shown in the discussion of the results (Sec. VII, B) how a comparison of these various quantities gives useful supplementary information.

---

* By comparison with Eqs. 17 and 18, it is seen that the definitions of $\overline{u'^2}$ and $\overline{v'^2}$ become: $\overline{u'^2} = \frac{n}{n-1} E(t)$ and $\overline{v'^2} = \frac{n}{n-1} F(t)$.

As has been indicated in sub-section D, "Standard Error of Calculated Velocities", the random errors in the velocity are all additive in effect in the computation of turbulence intensity. For example, if there were no turbulence the calculations would show

$$\frac{\sqrt{\overline{u'^2}}}{U} = 0.4\% \quad \text{and} \quad \frac{\sqrt{\overline{v'^2}}}{U} = 0.4\%,$$

as previously explained; but if there is actually a true turbulence intensity of 1%, then the analysis would yield

$$\frac{\sqrt{\overline{u'^2}}}{U} = \sqrt{1.0^2 + 0.4^2} = 1.08\%$$

and

$$\frac{\sqrt{\overline{v'^2}}}{U} = \sqrt{1.0^2 + 0.4^2} = 1.08\%$$

Consequently, it is apparent that the effects of the random analysis errors decrease rapidly as the true turbulence intensity increases. Except for the measurements made with no grid, the sampling errors are far more serious than the analysis errors.

H. Calculation of Correlation Coefficients

The Lagrangian correlation coefficients $r_u(\tau)$ and $r_v(\tau)$ were calculated for any time interval τ as the correlations between $u_i(-\tau/2)$ and $u_i(\tau/2)$, and $v_i(-\tau/2)$ and $v_i(\tau/2)$, respectively. Applying the standard statistical formula for correlation, the equations for calculating $r_u(\tau)$ and $r_v(\tau)$ are:

$$r_u(\tau) = \frac{\overline{u_i(-\tau/2)\, u_i(\tau/2)} - \overline{u}(-\tau/2)\, \overline{u}(\tau/2)}{\sqrt{\left[\overline{u_i(-\tau/2)^2} - \overline{u}(-\tau/2)^2\right]\left[\overline{u_i(\tau/2)^2} - \overline{u}(\tau/2)^2\right]}} \tag{31}$$

$$r_v(\tau) = \frac{\overline{v_i(-\tau/2)\, v_i(\tau/2)} - \overline{v}(-\tau/2)\, \overline{v}(\tau/2)}{\sqrt{\left[\overline{v_i(-\tau/2)^2} - \overline{v}(-\tau/2)^2\right]\left[\overline{v_i(\tau/2)^2} - \overline{v}(\tau/2)^2\right]}} \tag{32}$$

wherein all the variables are as previously defined. These equations are equivalent to the simpler definition of the Lagrangian correlation given by Eq. 6. Ideally, $\overline{v}(-\tau/2)$ and $\overline{v}(\tau/2)$ should be zero for perfectly balanced tracers, but because of small errors in the tracer density and sampling errors the values were never exactly zero. By inspection, it is obvious that these equations yield $r_u(0) = r_v(0) = 1$, as expected.

It may be noted that the calculation of the correlation coefficients for each τ value was based on only one pair of velocities from each trajectory; furthermore, for a given τ, these velocities were always taken at the positions corresponding to $t = -\tau/2$ and $t = \tau/2$ with $t = 0$ located near the center of the photographs, as previously explained. There were two reasons why this procedure was adopted:

1. The decay of turbulence undoubtedly affects the correlation coefficients. To keep this effect reasonably uniform, the velocities at the fixed times $t = -\tau/2$ and $t = \tau/2$ were used for calculating the correlations at time τ.

2. To get meaningful values of the correlation coefficients, they must be calculated from a sample of completely independent pairs of observations. Since on any one trajectory the velocities are correlated one to another over a long distance, it is impossible to take more than one pair of velocities from each trajectory without getting interdependent data. This is especially true for the larger values of τ, where the time intervals for any two pairs of velocity measurements from the same trajectory would have to overlap.

The necessity of using independent data is illustrated by the results of a previous study of this kind (Ref. 10). In that study complete correlation curves were computed for each individual trajectory by using a great many overlapping pairs of velocity measurements for each value of τ. The curves for individual trajectories were extremely varied, and were meaningless until averaged together.

A great saving of labor was effected by calculating the correlation coefficients only for selected values of τ. Although the positions of all the tracer images were measured on the photographic plates, the velocities

were calculated only for every sixth flash interval, except for some additional values near the center of the plate ($t = 0$). The values of τ used were 0, 2, 4, 6, 8, 12, 18, 24, 36, 48, 60, 72, 84, 92 and 100 flash intervals.

VI. OUTLINE OF EXPERIMENTS

Seven experimental setups were used in obtaining photographs of trajectories. The pertinent information for each set of trajectories is summarized in Table 1. The chronological order in which the data were obtained is as follows: I, II, IV, III, V, I', VI, where the Roman numerals designate the seven sets of data.

During the course of the experiments, the only major changes in experimental technique were those in the setup for injecting the tracers. First, for Sets I and II, the injector tip was attached to the downstream edge of the slender strut which extended from the top window down to a position 5/16 in. below the injector tip (or center of the tunnel). Since it was observed that the vortices shed from the end of the strut disturbed the tracers, the strut was extended down 3-5/16 more inches (Fig. 3) before Sets III and IV were made. Set V was then performed without any strut by using recirculated tracers, since it was then suspected that the strut itself still introduced appreciable turbulence. This was found to be the case, and the new injection system was devised with the injection needle mounted in the back of the center vertical bar of the grid. This setup was used for Sets I' and VI.

During the course of the experiments other small improvements in technique were made, such as in preparing tracers and measuring plates. Therefore, the quality of the results for the later sets should be considered slightly better than the earlier ones.

TABLE 1

Summary of Experimental Runs

	III	V	VI	II	IV	I	I'
Number of trajectories	15	11	27	34	35	25	15
Number of plates measured	6	7	11	22	22	11	11
Grid: mesh size, M, in.	none	none	1/2	1	2	1	1
bar diam., d, in.	none	none	1/8	1/4	1/2	1/4	1/4
Injector located in:	strut	none*	grid	strut	strut	strut	grid
Mean velocity of tracers: Horizontal component, U, cm/sec	48.9	49.7	48.1	49.9	49.7	147.2	148.5
Vertical component V, cm/sec	0.4	0.3	0.1	0.4	0.5	0.8	0.8
Water Temperature, ^{o}C:	28.3	28.2	25.7	21**	24**	18**	28.4
Reynolds number: UM/ν	-	-	6900	13000	27000	35000	45300
Average Turbulence Intensity:*** $\frac{\sqrt{\overline{u'^2}}}{U}$, %	1.38	0.60	2.63	3.41	4.11	3.27	2.76
$\frac{\sqrt{\overline{v'^2}}}{U}$, %	1.95	0.50	1.67	2.73	3.93	2.94	3.05

* The strut with the injector was removed after the tracers had been injected. The tracers were photographed after recirculating.

** Indicates temperature was estimated.

*** Root-mean-square of intensities at 15 standard t-values.

VII. EXPERIMENTAL RESULTS

The experimental results will be presented and discussed in three sections: Mean Velocities, Turbulence Intensity and Decay, and Lagrangian Correlations.

A. Mean Velocities

The instantaneous longitudinal and vertical components of the velocity of the tracers were determined from the photographic plates, as explained in the previous sections. The variation of these velocities with time has been illustrated in Fig. 6 for three typical trajectories from Set VI.

In general, the velocities were calculated only for time values $t = 0, \pm 1, \pm 2, \pm 3, \pm 4, \pm 6, \pm 9, \pm 12, \pm 18, \pm 24, \pm 30, \pm 36, \pm 42, \pm 46,$ and ± 50 in units of flash intervals. The average velocities $\overline{u}(t)$ and $\overline{v}(t)$ are plotted in Figs. 7 and 8 at the various t values for each set of trajectories.

The scatter of the points in Figs. 7 and 8 is related to the turbulence intensity. The scattering is to be expected because of the sampling process being utilized, and only a small part of it is attributable to experimental error. However, because the velocities at nearby positions are correlated one to another, the scatter of points does not appear completely random, but seems to indicate definite local ups and downs. If the experiments were repeated and a different sample of trajectories obtained, the ups and downs would be different. Consequently, in plotting the curves through the points, no attempt was made to follow the small oscillations, as it was believed that they had no significance.

Confidence limits for the plotted average velocities may be readily determined to show that the scatter is of a reasonable order of magnitude. The 95% confidence limits are defined in such a way that the probability is 95% that the true population mean will fall between the two 95% confidence limits established on the basis of a single sample of trajectories (or set) chosen at random to represent the infinite population. By assuming that the individual velocities are normally distributed, the student's t-distribution may be used to calculate the 95% confidence limits by the standard procedure found in any text of mathematical statistics (for example, Ref. 12). To simplify the calculation, the average turbulence intensity for

each set was used instead of the intensity at each individual time value. The results are summarized in Table 2. An inspection of Figs. 7 and 8 will show that the curves lie well within the 95% confidence limits for the mean velocity at practically all the points.

TABLE 2

Approximate 95% Confidence Limits for $\overline{u}(t)$ and $\overline{v}(t)$

(based on students' t-distribution and average turbulence intensities in Table 1)

Set	No. of Trajectories	Avg. $\sqrt{\overline{u'^2}}$ cm/sec	95% Confidence limits for $\overline{u}(t)$ cm/sec	Avg. $\sqrt{\overline{v'^2}}$ cm/sec	95% Confidence limits for $\overline{v}(t)$ cm/sec
III	15	0.67	$\overline{u}(t) \pm 0.37$	0.95	$\overline{v}(t) \pm 0.52$
V	11	0.30	$\overline{u}(t) \pm 0.20$	0.25	$\overline{v}(t) \pm 0.17$
VI	27	1.27	$\overline{u}(t) \pm 0.51$	0.80	$\overline{v}(t) \pm 0.32$
II	34	1.70	$\overline{u}(t) \pm 0.60$	1.36	$\overline{v}(t) \pm 0.48$
IV	35	2.04	$\overline{u}(t) \pm 0.70$	1.95	$\overline{v}(t) \pm 0.66$
I	25	4.81	$\overline{u}(t) \pm 1.97$	4.33	$\overline{v}(t) \pm 1.78$
I'	15	4.09	$\overline{u}(t) \pm 2.20$	4.53	$\overline{v}(t) \pm 2.49$

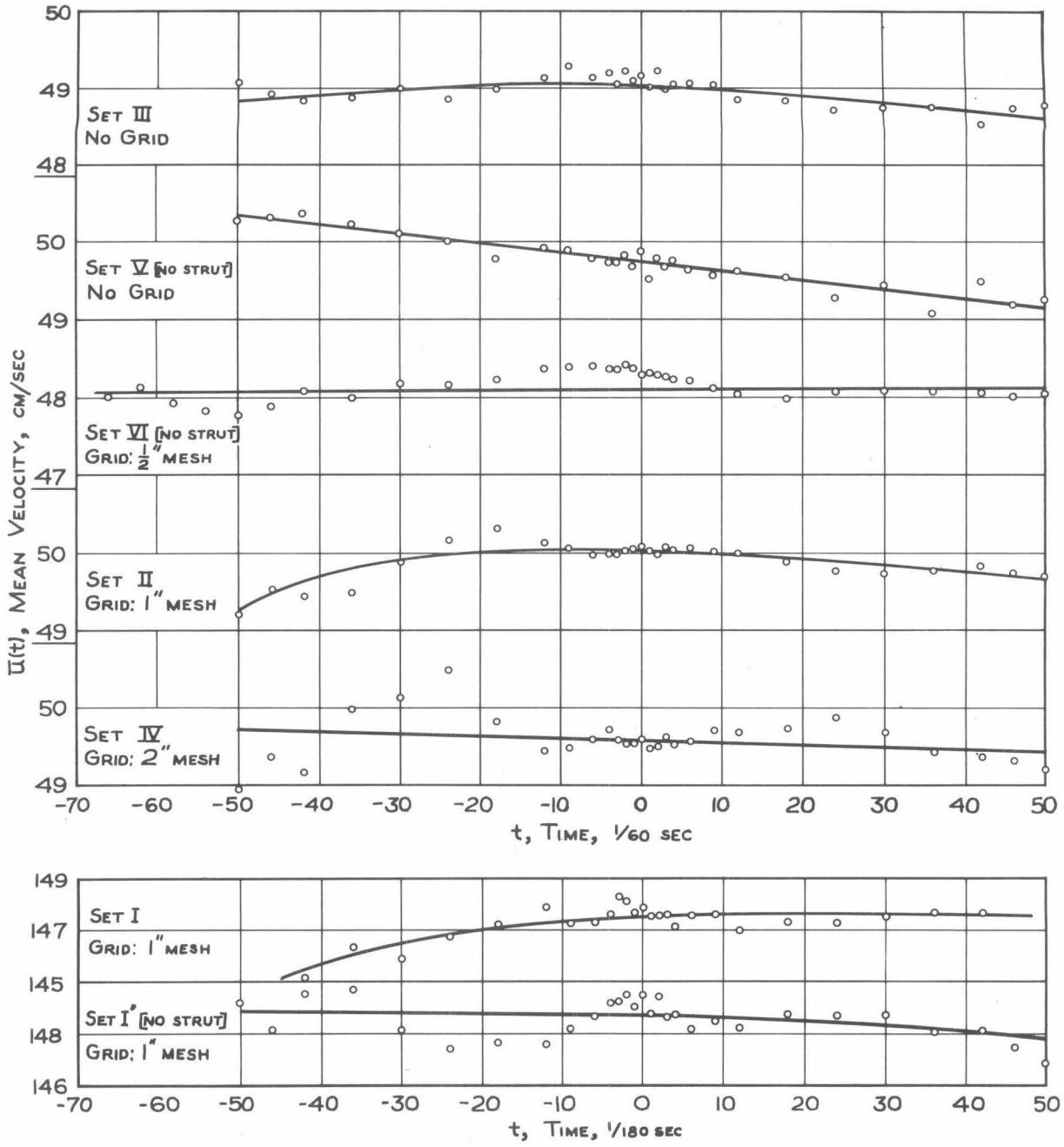

Fig. 7 - Mean longitudinal velocity, $\bar{u}(t)$, averaged over all trajectories in each set for various values of time t.

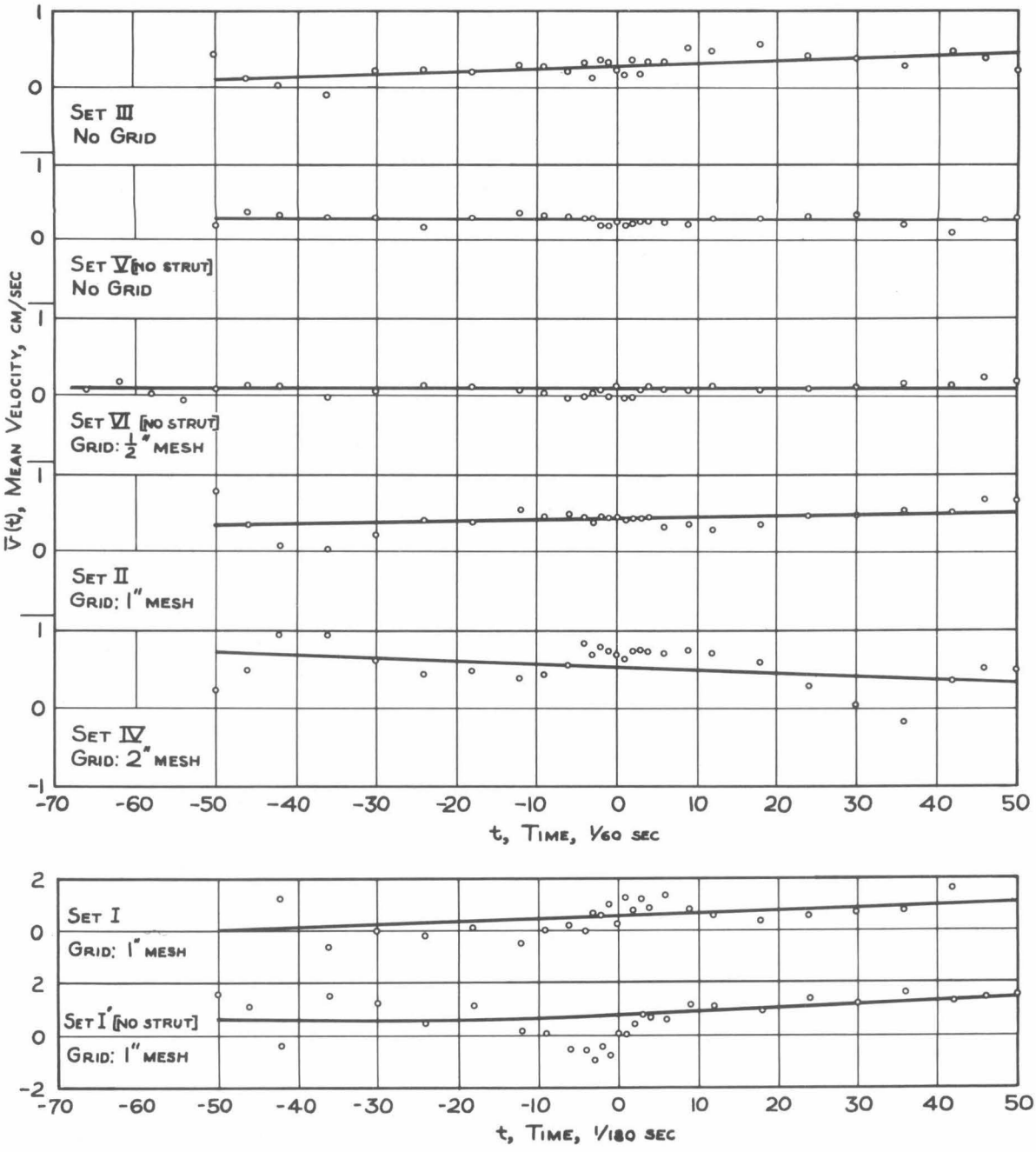

Fig. 8 - Mean vertical velocity, $\bar{v}(t)$, averaged over all trajectories in each set for various values of time t.

It may be noted (Fig. 7) that for Set V (no grid, no strut) the average velocity $\overline{u}(t)$ decreases steadily as t increases (i.e., going downstream). Apparently the rate of growth of the boundary layers is not sufficient to offset the flare in the working section, resulting in a net deceleration of the flow in the core. By contrast, Set III, also without grid, but with injector strut, does not show this same effect until the tracers pass the center of the field. The difference can only be attributed to the wake of the strut. In addition to reducing the mean velocity of the tracers, it will be seen in the next section that the strut also increases the turbulence level in its wake.

The strut effect may also be noted for sets with a grid by comparing $\overline{u}(t)$ curves for Sets I and I', which differ only in the injector setup. Set I shows a definite region of acceleration at the beginning, whereas Set I' (with no strut) does not. The same effect is noticeable in Set II, but hardly at all in Set IV because the turbulence, due to the large grid in this case, is more intense.

For the sets with a turbulence grid, there appears to be no significant deceleration along the working section as was observed in Set V. Since the Reynolds numbers (Ux/ν) are in the critical range for transition from laminar to turbulent boundary layer flow for values of x of the order of one foot, it is concluded that the boundary layer becomes turbulent when the flow is disturbed by a grid. In comparing the two cases, it is helpful to note that for potential flow in the working section the decrease in velocity between $t = -50/60$ and $t = +50/60$ sec when the average velocity is 49 cm/sec would be 4.6% or 2.3 cm/sec. For the case of the laminar boundary layer (Set V) the velocity decrease is only 1.1 cm/sec., showing that the flair of the tunnel is twice too much for this condition; moreover, it appears from the sets with grid that the effect of the turbulent boundary layer on the core velocity must be just about twice as great as that of the laminar boundary layer. This conclusion appears reasonable because it is well known that a turbulent boundary layer thickens more rapidly than a laminar one.

The curves of vertical velocity $\overline{v}(t)$ (Fig. 8) show that the mean velocity was slightly greater than zero for all sets, indicating that the tracers have a slow rate of rise superimposed on the turbulent motion. In spite of great care taken to obtain tracers of exactly the correct density, the loss

of carbon tetrachloride from the tracer mixture by volitizing in air and dissolving in water could not be completely controlled. Consequently, when the tracers were finally injected they tended to be slightly lighter than the water. Since the ratio of the average rising velocity V to the mean forward velocity U is always 1% or less, as shown in Table 1, the errors due to this undesirable rising tendency are considered unimportant.

Although some of the $\overline{v}(t)$ curves seem to indicate that the rising velocity is increasing or decreasing along the working section, these trends are not considered significant. (See confidence limits in Table 2.)

Average longitudinal and vertical velocities, $\overline{u}_i$ and $\overline{v}_i$, for individual trajectories were also calculated and are tabulated in Tables 3 and 4. In the tables the grouping of the trajectories on the photographic plates is indicated by the horizontal bars in each column; when no bar appears between adjacent entries, then the trajectories were measured from the same plate. At the bottom of the tables the standard deviations for $\overline{u}_i$ and $\overline{v}_i$ are listed for each set. It is remarkable that there is so much variation within each set, and an inspection of the plate grouping shows that even on single plates there can be wide variation in both the $\overline{u}_i$ and $\overline{v}_i$ values. This result is also vividly illustrated by Fig. 6, which shows that the difference between mean velocities of three trajectories on a single plate is large compared with the turbulent fluctuations of the velocity along a single trajectory. This variability of mean velocity was observed previously (Ref. 10) in similar experiments.

For Set V (no grid, no strut) the standard deviations $\sigma_{\overline{u}_i}$ and $\sigma_{\overline{v}_i}$ drop to very low values. Assuming that there is actually very little turbulence for this set, the values of $\sigma_{\overline{u}_i}$ and $\sigma_{\overline{v}_i}$ are indicative of the magnitude of the experimental errors. Therefore, the large variations in the average trajectory velocities for the sets with a turbulence grid must be attributable to the turbulence itself.

B. Turbulence Intensity and Decay

As indicated in Table 1, seven sets of measurements were made. Five of these sets were with turbulence-producing grids at the inlet to the working section and two were without grid. Of the two sets without grids, i.e., with free tunnel, one was made with and the other without the injector strut in the working section. Measurements of turbulence intensities

TABLE 3

Mean forward velocity $\bar{u}_i$ in cm/sec for individual trajectories based on 15 values of time t.

	SET						
No.	III	V	VI	II	IV	I	I'
1		49.6	47.8	50.8	47.9	148.5	147.3
2		49.8	49.0	51.8	49.7	142.8	149.4
3		49.7	46.6	51.8	50.0	151.7	149.0
4		49.7	48.5	47.8	46.5	143.1	144.1
5		49.8	48.2	49.7	50.5	144.9	149.8
6		50.0	48.3	51.7	50.2	149.0	148.3
7		49.6	48.2	51.1	49.4	150.7	151.5
8		49.6	47.8	52.8	50.0	147.1	147.8
9		49.9	50.1	48.4	50.7	145.2	148.8
10		49.9	48.8	49.2	50.2	145.1	153.3
11	49.4	49.7	49.2	51.7	51.4	154.3	149.7
12	48.9		48.5	50.5	50.0	151.2	145.8
13	49.3		47.0	51.4	47.7	144.4	148.5
14	48.7		48.3	50.4	50.1	147.6	147.2
15	48.9		46.2	48.1	49.7	145.8	146.8
16	48.5		50.4	48.9	48.5	149.6	
17	48.4		48.7	47.1	51.1	145.4	
18	49.0		47.4	49.4	51.6	147.1	
19	48.7		47.9	49.5	51.8	148.8	
20	49.5		47.4	50.6	48.8	140.9	
21	48.7		46.7	50.8	50.6	150.5	
22	48.8		49.3	49.6	49.5	146.0	
23	48.8		47.5	50.5	49.3	144.4	
24	49.4		49.1	49.2	48.2	149.6	
25	48.2		46.3	49.0	49.1	145.2	
26			47.5	50.2	49.2		
27			49.0	50.1	51.7		
28				47.6	51.4		
29				49.1	49.6		
30				50.5	51.4		
31				49.9	46.3		
32				48.9	50.2		
33				50.6	48.5		
34				48.2	51.5		
35					46.9		
Avg. = U	48.9	49.7	48.1	49.9	49.7	147.2	148.5
$\sigma_{\bar{u}_i}$	0.36	0.10	1.07	1.35	1.46	3.18	2.21
$\sigma_{\bar{u}_i}/U$	0.73%	0.20%	2.20%	2.70%	2.94%	2.16%	1.48%

Note: Each group of values between horizontal bars is from a single photograph.

TABLE 4

Mean vertical velocity $\bar{v}_i$ in cm/sec for individual trajectories, based on 15 values of time t.

	SET						
No.	III	V	VI	II	IV	I	I'
1		0.2	-0.8	0.0	0.0	-1.9	2.4
2		0.2	1.1	0.7	-0.3	6.2	1.6
3		0.4	0.1	0.0	-0.7	-1.3	1.7
4		0.4	-0.3	0.2	1.0	0.0	-1.6
5		0.2	0.2	0.7	0.3	0.7	3.8
6		0.3	-0.7	-0.5	-1.3	-0.4	-4.5
7		0.2	-0.1	-0.8	1.7	0.7	-3.0
8		-0.1	0.0	-0.5	0.1	3.3	0.6
9		0.2	0.0	-1.3	0.9	1.3	-2.2
10		0.4	-0.4	0.0	-0.1	-1.0	0.7
11	0.2	0.4	0.4	1.0	0.7	-0.7	2.2
12	0.6		0.7	0.3	1.9	0.2	4.8
13	1.4		0.2	-1.2	-1.7	2.0	-0.9
14	0.0		0.3	1.6	1.3	6.2	3.0
15	0.2		0.8	2.0	-0.1	1.6	3.5
16	-0.7		-0.3	0.7	1.0	0.6	
17	1.3		-0.1	-0.4	-1.8	5.2	
18	-1.1		-0.4	0.5	0.1	7.6	
19	1.1		-0.1	0.4	-0.5	-3.4	
20	-0.2		0.5	1.1	2.1	-1.6	
21	0.9		-0.1	2.1	0.5	-0.6	
22	1.1		1.0	1.0	2.8	0.0	
23	0.4		-0.4	2.2	-0.7	-4.3	
24	0.0		0.2	1.1	1.5	-1.6	
25	1.0		-0.2	1.7	2.1	2.7	
26			0.1	1.4	-0.6		
27			0.4	-1.0	1.3		
28				-0.8	1.2		
29				0.5	1.1		
30				-1.0	1.1		
31				-0.4	1.2		
32				0.2	-1.5		
33				0.4	-0.2		
34				0.3	1.2		
35					2.0		
Avg. = V	0.4	0.3	0.1	0.4	0.5	0.8	0.8
$\sigma_{\bar{v}_i}$	0.73	0.15	0.48	0.97	1.17	2.97	2.72
$\sigma_{\bar{v}_i}/U$	1.50%	0.30%	0.99%	1.94%	2.34%	2.02%	1.82%

Note: Each group of values between horizontal bars is from a single photograph.

$\sqrt{\overline{u'^2}}/U$ and $\sqrt{\overline{v'^2}}/U$ in the free tunnel are shown on Fig. 9. The intensities measured with the injector strut in the flow are seen to be significantly higher than those without the strut, although all other conditions of flow were the same for the two sets of measurements. Furthermore with the strut the intensities are seen to decrease appreciably with distance downstream, while without the strut the intensities do not vary with distance. One concludes from these results that the injector strut introduces appreciable turbulence. Reasoning along the lines followed in the analysis of measurement errors, (Sec. V, G) one would expect the strut effect to show up most clearly when the turbulence is lowest, as it is in the free tunnel.

The turbulence intensities $\sqrt{\overline{u'^2}}/U$ and $\sqrt{\overline{v'^2}}/U$ for Set V, with free tunnel without injector strut, are 0.60 and 0.50 percent, respectively, as shown in Fig. 10 and listed in Table 1. As explained in Sec. V, G, these measured values can be considered to be the square root of the sum of the squares of the actual intensity and the relative standard errors. If only the standard measurement errors of 0.4 percent in both the longitudinal and vertical components of the intensities are considered, the resulting turbulence intensities are 0.45 and 0.3 percent. Actually, there are other unavoidable errors due to such factors as variation in tracer droplet density and its effect on the settling or rising of the tracer, and variation in mean velocity due to slight fluctuations in pump speed. all of these errors tend to increase the observed turbulence velocity fluctuations and hence the measured intensities. This means that even the intensities of 0.45 and 0.3 percent, which have been corrected for measurement errors are high by some unknown amount. The fact that the turbulence intensities in the free tunnel without injector strut (Fig. 9) show no tendency to dissipate with distance downstream, may be taken as evidence that the errors are still an appreciable part of the measured result. This reasoning leads to the conclusion that the true turbulence intensities $\sqrt{\overline{u'^2}}/U$ and $\sqrt{\overline{v'^2}}/U$ are less, respectively, than 0.45 and 0.3 percent.

Figures 10 and 11 show the measured turbulence intensities in percent plotted as functions of distance from the turbulence grid for each of

the five sets of experiments in which grids were used. The individual measurements were made at fixed intervals of time from the reference position $t = 0$ rather than at fixed distances from the grid. The distances x in the above figures are calculated by Eq. 16. The curves shown in the figures have been fitted to the data by eye. With negligible exceptions, these curves fall well within the 95 percent confidence limits of the data, which limits can be calculated from information given in Table 5. The turbulence is seen to diminish with distance from the source.

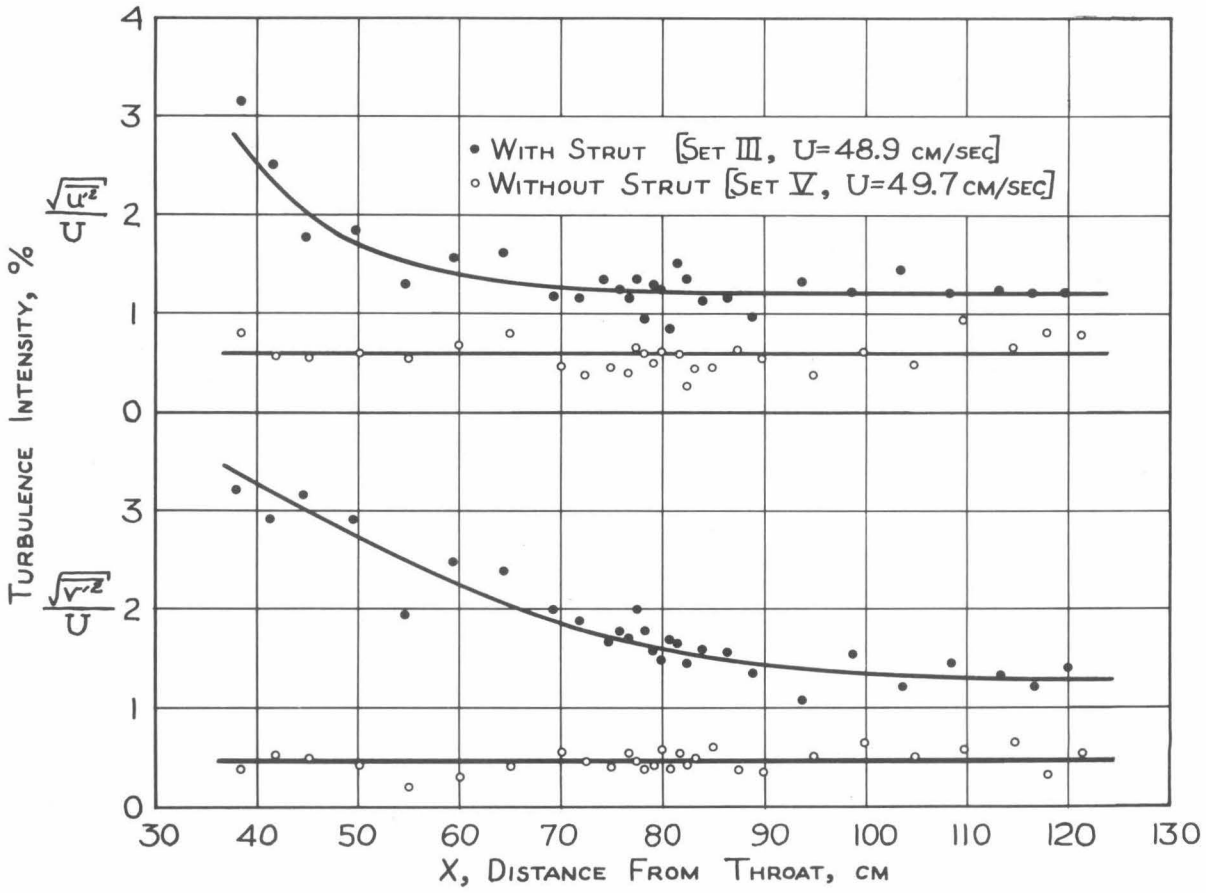

Fig. 9 - Turbulence intensities measured in the working section without turbulence grid, showing the effect of the injector strut. For Set III the centerline of the strut was 24.4 cm from the throat.

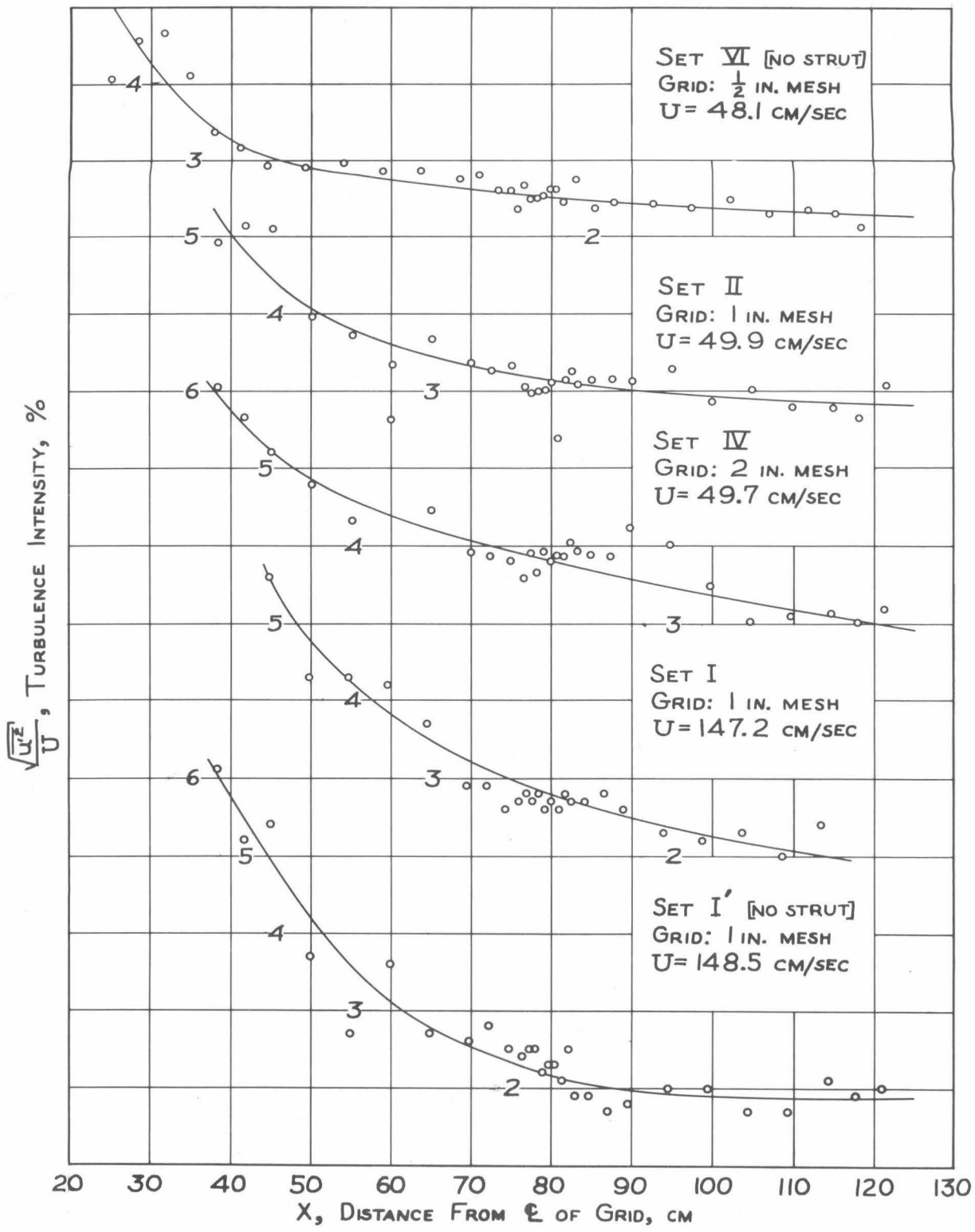

Fig. 10 - Longitudinal turbulence intensity, as a function of the distance from the grid, calculated from all the trajectories in each set.

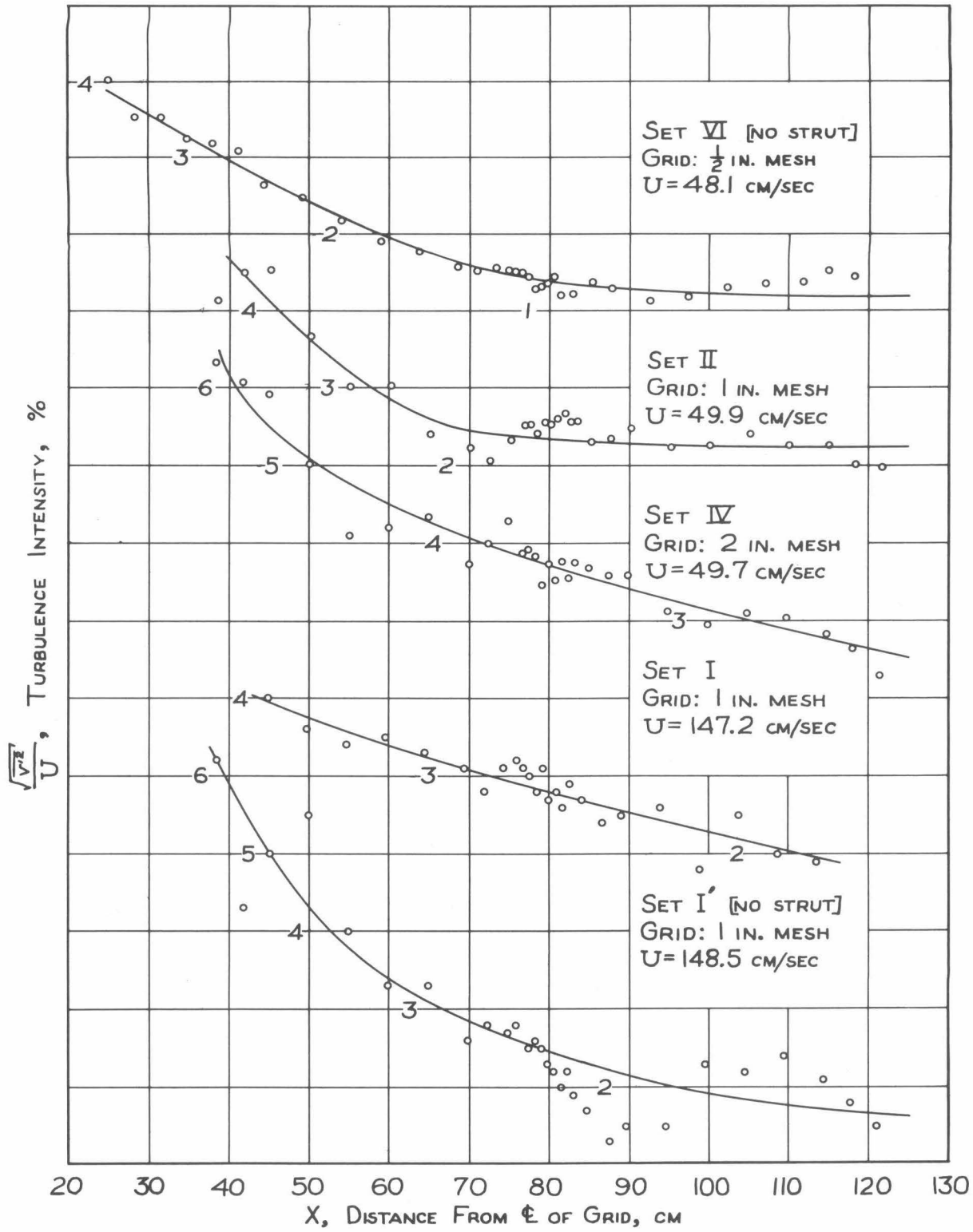

Fig. 11 - Vertical turbulence intensity as a function of the distance from the grid, calculated from all the trajectories in each set.

TABLE 5

95% Confidence Limits for Turbulence Intensities, $\sqrt{\overline{u'^2}}/U$ and $\sqrt{\overline{v'^2}}/U$.*

Set No.	No. of Trajectories	Ratio of lower confidence limit to observed value	Ratio of upper confidence limit to observed value
III	15	0.73	1.57
V	11	0.70	1.75
VI	27	0.78	1.37
II	34	0.80	1.31
IV	35	0.81	1.31
I	25	0.78	1.39
I'	15	0.73	1.57

All of the curves of Figs. 10 and 11 have been replotted on Fig. 12 using x/M instead of x for the abscissa where M is the mesh distance of the grid. On this figure one can compare the intensities in the longitudinal and vertical directions. Experiments in wind tunnels with grid-produced turbulence show that these two intensities are the same. From Fig. 12 it can be seen that $\sqrt{\overline{u'^2}}/U$ and $\sqrt{\overline{v'^2}}/U$ are very close to equal for Sets IV, I and I'. In Set II the two components of the intensities differ appreciably although the difference is not statistically significant at the 95 percent level over most of the range. In Set VI the two components of turbulence intensity differ widely. From this it appears that in only one of the five sets of measurements were the two components of turbulence intensity significantly different over a large part of the range.

It will be observed that tunnel conditions for Sets I and I' were the same except that in Set I the strut injector was used and in Set I' the injector was in the grid and the strut was removed. The fact that the difference between the measured intensities in these two sets is small,

* Based on chi-square distribution. See, for example, Ref. 13.

shows that the disturbance of the strut is of lesser importance when the turbulence intensity in the flow is appreciable.

On Figs. 13 and 14, the quantities $U^2/\overline{u'^2}$ and $U^2/\overline{v'^2}$, respectively, have been plotted against x/M. The lines on the graphs were fitted by eye to each set of data on a separate sheet and then transferred to the figures. Although there is appreciable scatter in the data, the straight lines appeared to fit them as well as any curve, thus agreeing with the form of Eq. 13. One striking feature of Figs. 13 and 14 is the wide range of slopes of the curves. Analysis and experience (Ref. 8) indicate that for similar grids, as was the case in the present experiments, the slopes of the curves should be the same except for some small effects of the grid Reynolds number, R_M, the values of which are listed in Figs. 13 and 14. The quantity b in Eq. 14, which is proportional to the slope, varies from 29 to 145 for the curves of Fig. 13, increasing with R_M and suggesting the existence of a large Reynolds number effect. With one exception (Set VI), the curves of Fig. 14 show the same systematic variation of b with R_M.

The data are of limited accuracy because of the errors inherent in the method of obtaining them. The sampling error is probably the largest of these due to the fact that the samples taken are relatively small. This error can be reduced by increasing the sample size; but this also increases the work and cost of a single set of runs and seriously limits the scope of any investigation. In spite of such inaccuracies of the data, it appears that the conclusions already outlined are justified.

Referring to Eqs. 19 to 30, it is seen that the mean turbulent energies E and F can be arrived at in two ways as expressed by Eqs. 29 and 30. The first of these, as illustrated by the left-hand sum in Eq. 29, considers the effect of the velocity fluctuations along a trajectory relative to the average $\overline{u}_i$ of that trajectory as expressed by Eq. 23, and then the effect of the variation of the individual trajectory averages $\overline{u}_i$ from the grand average U as in Eq. 27. The second way involves calculating the intensities at given times, t, using all trajectories (Eq. 21), then averaging over t, and finally adding the variance of $\overline{u}(t)$ (Eq. 25). By comparing the magnitudes of the quantities in Eqs. 29 and 30, it is possible to see the relative effects upon the turbulence of the velocity fluctuations within a trajectory and of the fluctuations of the mean velocities from the grand average.

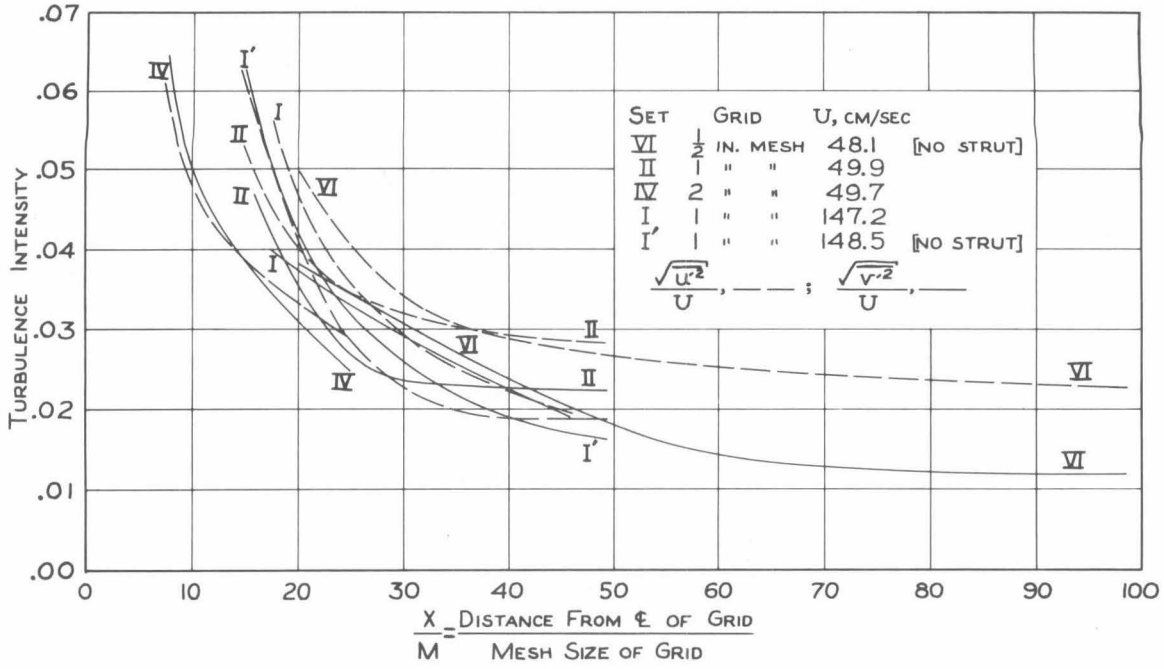

Fig. 12 - Composite of turbulence intensity curves for all sets with grid, as a function of the distance from the grid in mesh spacings. The curves are the same as those shown in Figs. 10 and 11, except for changes in the abscissa.

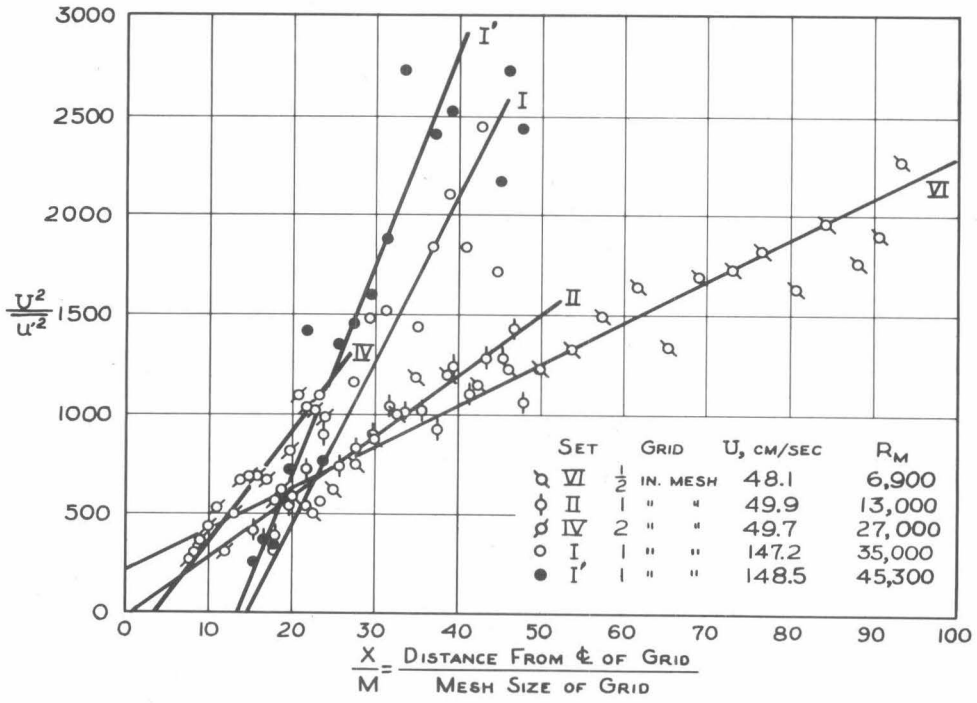

Fig. 13 - Decay of the longitudinal component of turbulence.

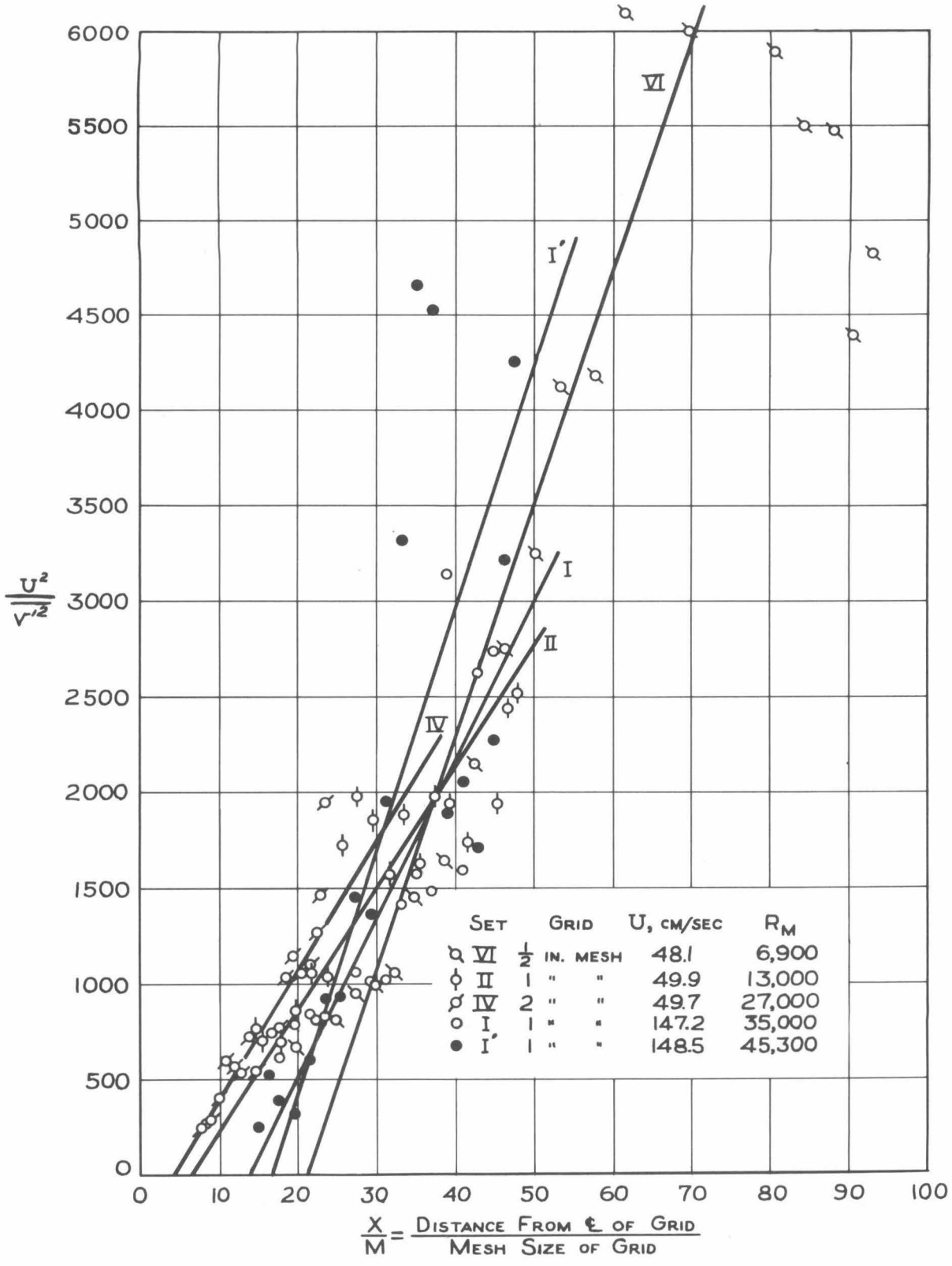

Fig. 14 - Decay of the vertical component of turbulence.

Analysis of the data from the five sets of experiments made with turbulence grid shows that from 30 to 70 percent of the mean turbulence energy E was contributed by the term $\sigma_{\overline{u}_i}^2$ in Eq. 29, which gives the *effect of the* variation of mean trajectory velocity $\overline{u}_i$. The term $\sigma_{\overline{u}(t)}^2$ which expresses the energy contribution of the fluctuation of the mean velocity $\overline{u}(t)$ from the grand average U amounted to less than 3 percent of the total energy E. The fact that this is small can be seen from Fig. 8. Analysis of the components of the energy F as expressed by Eq. 30 showed that $\sigma_{\overline{v}_i}^2$ ranged from 35 to 50 percent of F and that $\sigma_{\overline{v}(t)}^2$ was less than 2 percent of F. These results indicate that a large part of the measured turbulence energy results from the variation of the mean trajectory velocities.

An examination of the data for Set VI showed that the average energies $\overline{E}_i$ and $\overline{F}_i$ for individual trajectories differ by only 15 percent. On the other hand, the quantity $\sigma_{\overline{u}_i}^2$ was about 5 times as large as $\sigma_{\overline{v}_i}^2$ showing that the unusually high values of the intensity $\sqrt{\overline{u'^2}}/U$ (see Figs. 12 and 13) is due to the large value of $\sigma_{\overline{u}_i}^2$. Since $\sqrt{\overline{u'^2}}/U$ for Set VI is so different from that for the other sets, one is inclined to conclude that it is in error and to disregard it. On the other hand, the experiments of Set VI were made at the very end of the program using techniques that had been continually improved during all of the other tests and the results are thought to be more reliable than those obtained earlier.

C. Lagrangian Correlations

In Section III it was shown that the diffusion coefficient in a field of homogeneous isotropic turbulence is equal to the product of the turbulent energy $\overline{v'^2}$ and the integral of the Lagrangian correlation coefficient (cf. Eq. 9). Consequently, it was of interest to calculate the Lagrangian correlation coefficients, $r_u(\tau)$ and $r_v(\tau)$, for various values of the time lapse τ for the u and v velocities, respectively. Figures 15 and 16 show the results obtained by the procedure previously outlined in Section V, H. The curves plotted were fitted to the calculated points by eye with an effort to draw smooth curves without significant reverse curva-

ture. In the vicinity of $\tau = 0$, it is not possible to determine the shape of the curves because the flash interval over which the velocities are averaged becomes large compared with time lapse τ. Theoretically, the curves should have zero slope at $\tau = 0$.

As in the previous calculations the sampling error is inevitably large so that the large scatter of the points is believed to be of no particular significance. Naturally, the exact position of the curves is open to some question for the same reason, but the general trend should be indicative of the true situation.

Table 6 gives a partial tabulation of the 95 percent confidence limits for the true correlation based on the computed correlation for one sample size ($n = 25$). The figures in the table were obtained from curves in Ref. 13, which in turn were derived by David from the frequency distribution for the correlation coefficient of samples. As the sample size increases, the confidence interval becomes smaller, but very slowly. From Table 1 it is seen that the sample size (number of trajectories) ranges from 15 (Set I') to 35 (Set IV), excluding the sets with no grid. Hence, the confidence limits given for $n = 25$ are indicative of the order of magnitude of the sampling errors involved. It is of interest to note (Ref. 13) that even if 100 trajectories had been measured for each set, the confidence limits for a sample correlation of 0.50 are still widely spread, being 0.34 and 0.63 (compared with 0.13 and 0.74 when the sample size is 25). Consequently, by the tracer method hundreds of trajectories would have to be analyzed to get an accurate estimate of the true correlation; the labor involved would be tremendous.

In spite of these limitations, the data still show some interesting results in a qualitative way. In the first place, only 4 out of 10 curves in Figs. 15 and 16 cross the zero correlation line and reach negative correlations in the range of τ-values shown. Of these four, the r_v-curve for Set VI crosses at the smallest value of τ, namely about 50 flash intervals or 0.8 sec. The fact that the positive correlation persists over such a long time interval shows that the time scale must be large; or, in other words, if a tracer is moving faster than average as it enters the field of view, its velocity more likely than not will still be faster than average when it leaves. This checks the previous observation that a large part of the turbulent energy is attributable to the variation in mean velocity between trajectories. (Cf. Tables 3 and 4 and Sec. VII-B; also Ref. 10.)

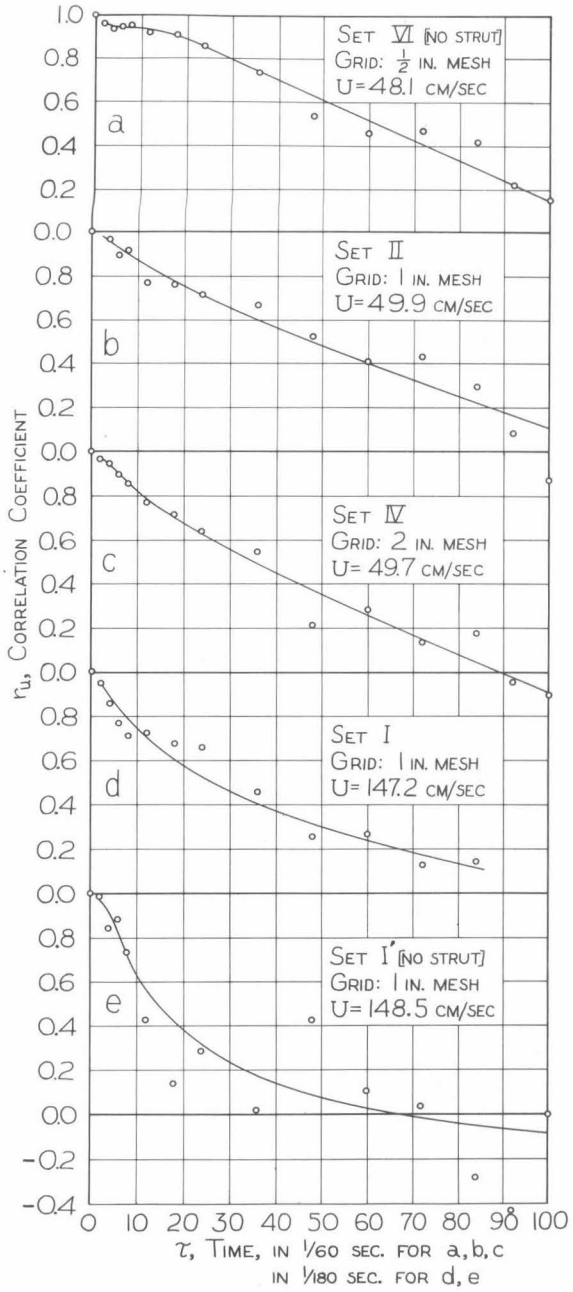

Fig. 15 - Lagrangian correlation coefficients for the longitudinal velocity fluctuations.

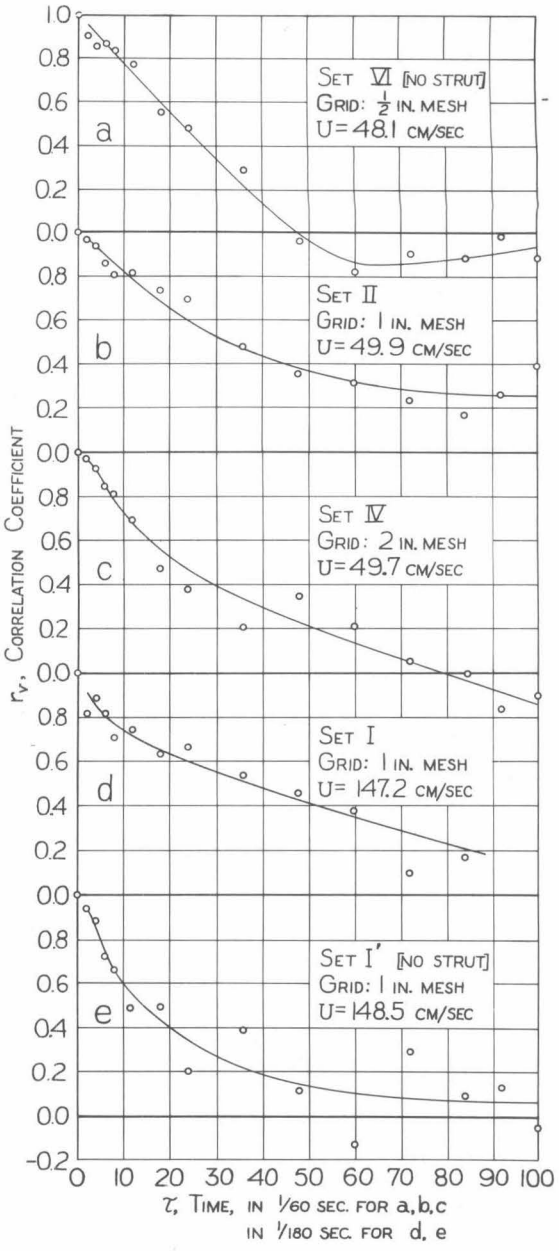

Fig. 16 - Lagrangian correlation coefficients for the vertical velocity fluctuations.

Furthermore, for Sets I and I', where the mean velocity is for all practical purposes three times that of the other sets, expansion of the time scale by a factor of three in the correlation graphs, as done in Figs. 15 and 16, results in curves which have practically the same appearance as the ones for the lower velocities. If this is true, in general, then the

TABLE 6

95% Confidence Limits for r_u and r_v for Sample of 25 Trajectories

r_u or r_v (computed value)	95% confidence limits for true value	
	lower	upper
0.00	-0.39	0.39
0.10	-0.30	0.47
0.20	-0.21	0.54
0.30	-0.10	0.61
0.40	0.00	0.68
0.50	0.13	0.74
0.60	0.26	0.80
0.70	0.41	0.85
0.80	0.58	0.90
0.90	0.77	0.95
1.00	1.00	1.00
For negative correlations, reverse all signs in the table.		

integral of the Lagrangian correlation

$\int_o^T r_v(\tau)\, d\tau$ for T large is inversely proportional to the velocity U for identical flow systems and grids. If it is further assumed that $\overline{v'^2}/U^2$ does not vary with velocity, then the diffusion coefficient as given by Eq. 9 is proportional to the mean velocity U. If the time factor $(T - T_o)$ in Eq. 11, is taken as inversely proportional to U, the amount of spreading of particles, $\overline{y^2}$, for a given forward movement (UT) of the fluid mass is unchanged. This is equivalent to stating that the turbulence is approximately kinematically similar regardless of the mean velocity for the geometrically similar grids used. There is undoubtedly a Reynolds number effect but it does not seem to obscure the basic similarity.

Because of the large values of the time required to make the correlation curves become effectively zero, no attempts were made to estimate the total areas under the correlation curves, which are required to obtain the diffusion coefficients (Eq. 9). For any future program, experimental apparatus should be developed to obtain much longer trajectories.

Another difficulty with obtaining the diffusion coefficient experimentally by integrating the correlation curves is the fact that it is impossible to achieve a homogeneous field of turbulence, as was assumed in the development of the theory. The continual decay of energy downstream from the grid undoubtedly has some effect on the correlation curves, but the nature of this effect is not clear. Possibly Set VI, with the smallest grid, is least affected by the decay because the rate of decay with distance is the smallest. However, the variation of intensity is at least partially compensated for by using the product of the intensities at $t = -\tau/2$ and $t = +\tau/2$ in the denominators of the formulas for $r_u(\tau)$ and $r_v(\tau)$ (Eqs. 31 and 32).

A comparison of the r_u and r_v curves does not show any consistent differences between the two groups of curves. Theoretically, there is reason to expect them to be identical. Subtracting the mean motion of the fluid from the total motion of the particle leaves only the turbulent motion. If this turbulence field is homogeneous and isotropic, then during an interval of time τ the displacement of a particle is random in both magnitude and direction. Consequently, the Lagrangian correlation must be the same for any component of velocity.

For Set I', the two correlation curves $r_u(\tau)$ and $r_v(\tau)$ are practically the same; furthermore, for Set I, r_v is only slightly larger than r_u (by 0.1 or less); and for Sets II and IV, r_v is generally slightly smaller than r_u (by 0.15 or less). Considering the confidence limits, these differences are not considered important, but for Set VI there is a marked difference between the curves; for example, for $\tau = 60/60$ sec, $r_u = +0.52$ and $r_v = -0.14$. Actually, the confidence intervals for these two figures still overlap slightly. In Sec. VII, B, it was noted that Set VI, for some unknown reason, is the only case where the standard deviations of the mean trajectory velocities $\overline{u}_i$ and $\overline{v}_i$ are greatly different (Tables 3 and 4). Since $\sigma_{\overline{u}_i} = 1.07$ and $\sigma_{\overline{v}_i} = 0.48$, the variations in $\overline{u}_i$ are rela-

tively more important in the over-all turbulence than the variations in $\overline{v}_i$; therefore, there is a stronger tendency for the u velocity of a tracer to remain slow or fast over a long period than for the v velocity. It does seem reasonable then that r_u should be larger than r_v, as was found.

In a previous study (Ref. 10), it was found that r_v was less than r_u for all values of τ for which the average correlation coefficients were calculated. The difference was as much as 0.4 for some τ-values. However, since the computation procedure was different (see Sec. V, H), the results are not directly comparable.

A comparison of Sets I and I' shows the effect of the injector strut, although coupled with an undetermined sampling error. The r_u-curve for Set I' is as much as 0.2 less than for Set I, and the r_v-curve is as much as 0.3 less. Since in both Sets I and I', r_u and r_v differ but slightly from each other, the difference between r_u and r_v, noted above for Set VI, cannot be attributed to having the injector in the grid instead of in the strut. The general effect of the strut is probably to make both the correlation coefficients larger than they should be, because the wake of the strut introduces some nonrandom components into the tracer motion.

If the Lagrangian correlation coefficients are known, and the turbulence field is assumed to be homogeneous and isotropic, then the power spectrum $F(\eta)$ and the time scale θ can be calculated by integration. By definition of the power spectrum, the quantity $F(\eta)\,d\eta$ is the fraction of the total energy associated with the frequency band η to $\eta + d\eta$. Kampe de Feriet has shown that

$$F(\eta) = 4 \int_0^\infty r(\tau) \cos(2\pi\eta\tau)\, d\tau,$$

where $r(\tau)$ is the correlation coefficient for any one of the velocity components. (See, for example, Ref. 14). A characteristic time, or time scale, is given as

$$\theta = \int_0^\infty r(\tau)\, d\tau.$$

Because of the uncertainty about the correlation curves, and the shortness of the trajectories, it was not possible to calculate the spectrum and the time scale except in a very rough way. From the correlation

curves it is easily seen that the time scale is of the order of one second for Sets VI, II, and IV, and about 1/3 as much for Sets I and I'. Approximate calculations also showed, as expected, a preponderance of energy in the low frequencies with insignificant energy for $\eta > 10$ cps.

A brief visual study of the tracer motion was made by taking motion pictures of clouds of tracers at 64 frames per second with a mean tunnel velocity of 50 cm/sec. The mean motion of the clouds was followed by turning the camera. From the motion pictures it was apparent that the turbulent motions were smooth and gradual, with a fairly large scale (of the order of several centimeters), and that there were no significant oscillations of high, or even medium , frequencies. Representative frequencies appeared to be of the order of one cycle per second. The lack of high frequency components is also quite evident in Fig. 5, which shows that the curvature of the trajectories is quite small and the spacing between images is surprisingly uniform.

VIII. CONCLUSIONS

1. The mean longitudinal velocity of particles of fluid as indicated by tracers varies appreciably from particle to particle where the mean velocity is observed over distances of about 3 ft. Variations of as much as 10 percent in the mean longitudinal velocity were observed between simultaneous observations on a single photograph, and variations of 5 percent were not uncommon. The mean vertical velocity of the tracers also varied considerably.

2. The variation in mean velocities of the tracers accounted for a large part of both the longitudinal and vertical components of the turbulence intensity.

3. Within 100 mesh lengths downstream from the grid the turbulence decays in such a way that $1/\overline{u'^2}$ and $1/\overline{v'^2}$ increased linearly with distance from the grid. This result agrees with findings of studies in wind tunnels.

4. The constant of proportionality "a" in Eq. 13, between the reciprocals of the turbulence energy and distance from the grid producing the turbulence,

varies strongly with grid Reynolds number. This differs from results of studies in wind tunnels which indicate that the variation of the constant of proportionality with Reynolds number is small.

5. With one exception, the five sets of measurements with turbulence grid indicate that the turbulence intensities $\sqrt{\overline{u'^2}}/U$ and $\sqrt{\overline{v'^2}}/U$ in a given flow are not significantly different.

6. The two correlation curves $r_u(\tau)$ and $r_v(\tau)$ were significantly different only for Set VI, where r_u was considerably larger than r_v over most of the range of τ-values used.

7. From the correlation curves and visual observations, it was apparent that most of the turbulent energy was associated with very low frequencies (of the order of 1 cps) and that the time scale was fairly large (of the order of 1 sec).

8. In making future studies of turbulence, it is recommended that observations be made over longer distances than in the present study. This is especially important if diffusion coefficients and spectra are to be determined from Lagrangian correlation coefficients.

9. A very large number of trajectories must be analyzed to make the sampling errors in the intensities and correlations reasonably small. Consequently, the tracer technique of studying turbulence in water is limited at present by the laborious procedures involved. Before it can be used extensively, it must be developed to the point where measurements can be taken with less expenditure of time than at present. On the other hand, there is no other way in which Lagrangian correlations can be experimentally determined.

10. The turbulence intensities $\sqrt{\overline{u'^2}}/U$ and $\sqrt{\overline{v'^2}}/U$ in the free tunnel were less, respectively, than 0.45 and 0.3 percent.

11. Disturbances introduced into the flow by devices, such as the injector strut used in the present investigation, cause appreciable errors in the velocity, turbulence, and correlation measurements. The errors in the turbulence measurements are largest when the turbulence is low, as it was in the free tunnel.

12. The flare of the working section is greater than necessary to accommodate a laminar boundary layer, so that with a laminar layer the mean velocity decreases in the downstream direction and the pressure increases. With a turbulent boundary layer, the flare in the working section is approximately correct and the mean velocity along the working section is very nearly uniform.

13. Tracer droplets containing carbon tetrachloride lose this constituent by evaporation in air and dissolving in water, making it difficult to maintain the correct density. In the present experiments the tracers were usually slightly too light and had a small rate of rise superimposed on the turbulent motion.

IX. ACKNOWLEDGMENTS

Important contributions to this investigation were made by a number of research workers who participated in the program at various stages. Professor A. C. Ingersoll carried out many of the calibration studies, and Mr. Edison R. Hoge developed much of the photographic technique. Mr. Freddy Storrer formulated the procedure for analysis of the data and performed many of the early experiments. Mr. George Nomicos assisted with the experimental work and made a study of the spectrum and the performance of the damping screens. During the latter part of the project Mr. Hugh S. Bell, Jr., performed the experiments, supervised the calculations, and prepared the figures for this report. The writers would like to express their thanks and appreciation to all the above-mentioned for their valuable services to the project.

BIBLIOGRAPHY

1. Jeans, J., "An Introduction to the Kinetic Theory of Gases," Cambridge University Press, p. 199, 1940.

2. Einstein, A., Ann. d. Physik, Vol. 17, p. 549, 1905.

3. Taylor, G. I., "Diffusion by Continuous Movements," Proc. London Math. Society, Vol. 20, p. 196, 1921.

4. Burgers, J. M., "On Turbulent Fluid Motion," Report No. E-34.1, Hydrodynamics Laboratory, Calif. Inst. of Tech., July 1951.

5. Dryden, Hugh L., "A Review of the Statistical Theory of Turbulence," Quarterly of Applied Math., Vol. 1, No. 1, p. 7, April 1943.

6. Taylor, G. I., "Some Recent Developments in the Study of Turbulence," Proc. 5th International Congress for Applied Mech., Cambridge, Mass., 1938.

7. Batchelor, G. K. and Townsend, A. A., "Decay of Isotropic Turbulence in the Initial Period," Proc. Royal Soc. (A), Vol. 193, p. 539, 1948.

8. Batchelor, G. K., "The Theory of Homogeneous Turbulence," Cambridge University Press, pp. 133-138, 1953.

9. Vanoni, Vito A., Hsu, En-Yun, and Davies, R. W., "Dynamics of Particulate Matter in Fluid Suspensions," Hydrodynamics Laboratory, Calif. Inst. of Tech., Report No. 71.1, Nov. 1950.

10. Vanoni, Vito A., and Hsu, En-Yun, "The Dynamics of Particulate Matter in Fluid Suspensions," Hydrodynamics Laboratory, Calif. Inst. of Tech., Report No. E-34, Dec. 31, 1951. See also Amer. Soc. of Civil Engineers Preprint 67, Chicago Centennial, 1952.

11. Knapp, R. T., Levy, J., O'Neill, J. P. and Brown, F. B., "The Hydrodynamics Laboratory of the California Institute of Technology," Trans. Amer. Soc. of Mech. Engrs., p. 442, July 1948.

12. Hoel, P. G., Introduction to Mathematical Statistics, 2nd Edition, Wiley, 1954.

13. Dixon, W. J., and Massey, F. J., Jr., "Introduction to Statistical Analysis", McGraw Hill, 1951.

14. Frenkiel, F. N., "On the Kinematics of Turbulence", Journal of the Aero. Sc., Vol. 15 (1948), pp. 57-64.